5

Snow and Snowmelt

Over much of the world's land areas, a significant portion of precipitation falls as snow and is stored on the surface for periods of time ranging from hours to months before melting and continuing through the land phase of the hydrologic cycle. (See Figure 3-21.) In many of these areas, snowmelt is the main source of surface-water supply (Figure 3-26) and ground-water recharge and the main cause of flooding.

The goal of this chapter is to develop an understanding of the hydrologically important aspects of snow and snowmelt. Following an examination of the nature of snow as a material and of techniques for the measurement of snow and snowmelt, we survey the distribution of snow at various scales and the role of snow in the hydrologic cycle. We then discuss the processes that control the melting of snow (relying extensively on the physical principles discussed in Appendix D) and the ways in which meltwater moves through the snowpack to the ground surface. An understanding of these processes is the basis for models used to predict and forecast snowmelt runoff and, next, we review approaches to and results of snowmelt modeling. The chapter concludes with a brief discussion of water-quality aspects of snowmelt.

5.1 MATERIAL CHARACTERISTICS OF SNOW

5.1.1 Snow Properties

Snow is a granular porous medium consisting of ice and pore spaces. When the snow is **cold** (i.e., its temperature is below the melting point of ice, 0 °C), the pore spaces contain only air (including water vapor). At the melting point, the pore spaces can contain liquid water as well as air, and snow becomes a three-phase system.

Consider a representative portion of a snowpack of height (depth) h_s and area A (Figure 5-1). Using the symbols M to designate mass, V for volume, h for height, and ρ for mass density; and the subscripts s for snow, i for ice, w for liquid water, m for water substance (liquid water plus ice), and a for air; we can define quantities that are useful in characterizing a snowpack. The snow volume is

$$V_s = V_i + V_w + V_a = h_s \cdot A. \qquad (5\text{-}1)$$

The **porosity,** ϕ, is defined as the ratio of pore volume to total volume:

$$\phi \equiv \frac{V_a + V_w}{V_s}; \qquad (5\text{-}2)$$

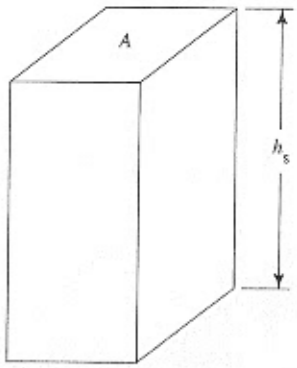

FIGURE 5-1
Dimensions of a representative portion of a snowpack, used in defining snowpack properties. A is the area of the upper surface; h_s is the snow depth.

therefore,

$$V_i = (1 - \phi) \cdot V_s. \tag{5-3}$$

The **liquid-water content,** θ, is defined as the ratio of the volume of liquid water in the snowpack to the total volume of snow:

$$\theta \equiv \frac{V_w}{V_s}. \tag{5-4}$$

Snow density, ρ_s, is defined as the mass per unit volume of snow, so

$$\rho_s = \frac{M_i + M_w}{V_s} = \frac{\rho_i \cdot V_i + \rho_w \cdot V_w}{V_s}. \tag{5-5}$$

Combining Equations (5-2)–(5-5) allows us to relate density, liquid-water content, and porosity as

$$\rho_s = (1 - \phi) \cdot \rho_i + \theta \cdot \rho_w, \tag{5-6}$$

where $\rho_i = 917$ kg m^{-3} and $\rho_w = 1000$ kg m^{-3}.

For the hydrologist, the most important property of a snowpack is the amount of water substance it contains, because this is the amount of water that will ultimately enter the land phase of the hydrologic cycle. This amount is called the **water equivalent** of the snowpack, and it is expressed as the depth of water that would result from the complete melting of the snow in place, h_m. Thus

$$h_m \equiv \frac{V_m}{A}, \tag{5-7}$$

where V_m is the volume of water resulting from the complete melting of the snow.

To relate the water equivalent to previously defined quantities, we note that

$$V_m = V_w + V_i \cdot \frac{\rho_i}{\rho_w}. \tag{5-8}$$

Substituting Equations (5-3) and (5-4) into Equation (5-8) yields

$$V_m = \theta \cdot V_s + (1 - \phi) \cdot V_s \cdot \frac{\rho_i}{\rho_w}. \tag{5-9}$$

We can now use Equations (5-1) and (5-7) to rewrite Equation (5-9) as

$$h_m = \theta \cdot h_s + (1 - \phi) \cdot h_s \cdot \frac{\rho_i}{\rho_w}, \tag{5-10}$$

$$= \left[\theta + (1 - \phi) \cdot \frac{\rho_i}{\rho_w}\right] \cdot h_s. \tag{5-11}$$

Finally, we see from Equation (5-6) that Equation (5-11) can be written as

$$h_m = \frac{\rho_s}{\rho_w} \cdot h_s. \tag{5-12}$$

In words, Equation (5-12) is often expressed as "water equivalent equals density times depth," where density is understood to mean relative density (i.e., specific gravity). This relation is used in snow-course measurements. (See Example 5-1.)

5.1.2 Snowpack Metamorphism

The density of new-fallen snow is determined by the configuration of the snowflakes, which is largely a function of air temperature, the degree of supersaturation in the precipitating cloud (Mellor 1964), and the wind speed at the surface of deposition. Higher wind speeds tend to break snowflakes that formed in stellar or needle-like shapes and to pack them together into denser layers. Observed relative densities (ρ_s/ρ_w) of freshly fallen snow range from 0.004 to 0.34 (McKay 1970), with the lower values occurring under calm, very cold conditions and higher values accompanying higher winds and higher temperatures. However, the usual range is 0.07 to 0.15 (Garstka 1964). Because of the difficulty of measuring the density of new snow, an average relative density of 0.1 is often assumed to apply when converting snowfall observations to water equivalents in the United States. The user of water-equiva-

lent data should be aware of the potential for significant errors in estimates based on an assumed density (Goodison et al. 1981).

As soon as snow accumulates on the surface, it begins a process of metamorphism that continues until melting is complete. Four mechanisms are largely responsible for this process: (1) gravitational settling, (2) destructive metamorphism, (3) constructive metamorphism, and (4) melt metamorphism.

Gravitational settling in a given snow layer takes place at rates that increase with the weight of the overlying snow and the temperature of the layer and decrease with the density of the layer. According to relations given by Anderson (1976), one could expect gravitational settling to increase density at rates on the order of 2 to 50 kg m^{-3} day^{-1} in shallow snowpacks. On glaciers, the pressure of thick layers of accumulating snow is the principal factor leading to the formation of solid ice.

Destructive metamorphism occurs because vapor pressures are higher over convex surfaces with smaller radii of curvature, so the points and projections of snowflakes tend to evaporate, and the vapor deposits on nearby less convex surfaces. These events lead to the formation of larger, more spherical snow grains with time. This process occurs most rapidly in snowflakes that have recently fallen, causing the density of a new-snow layer to increase at about 1% per hour. The process ceases to be important when densities reach about 250 kg m^{-3} (Anderson 1976).

Constructive metamorphism is the most important pre-melt densification process in seasonal snowpacks. Over short distances, this process occurs by **sintering,** in which water molecules are deposited in concavities where two snow grains touch, gradually building a "neck" between adjacent grains. Over longer distances, constructive metamorphism can occur as a result of vapor transfer within a snowpack due to temperature gradients; sublimation occurs in warmer portions of the snowpack, and the water vapor moves toward colder portions where condensation occurs. Very cold air overlying a relatively shallow snowpack often produces a strong upward-decreasing temperature gradient within the snow, with a concomitant upward-decreasing vapor-pressure gradient. Under these conditions, snow near the base of the pack evaporates at a high rate, often resulting in a basal layer of characteristic large planar crystals with very low density and strength called **depth hoar.**

Melt metamorphism occurs via two processes. In the first, liquid water formed by melting at the surface, or introduced as rain, freezes within the cold snowpack. This process results in densification and may produce layers of essentially solid ice that extend over long distances. The freezing at depth also liberates latent heat, which contributes to the warming of the snowpack and the acceleration of vapor transfer. The second metamorphic process accompanying melt is the rapid disappearance of smaller snow grains and growth of larger grains that occurs in the presence of liquid water. Because of this phenomenon, an actively melting snowpack is typically an aggregation of rounded grains the size of coarse sand (1 to 2 mm in diameter) (Colbeck 1978).

Except for the temporary formation of depth hoar, all the processes of metamorphism lead to a progressive increase in density through the snow-accumulation season (Figure 5-2). Figures 5-3 and 5-4 depict the regional variation in average seasonal snowpack density in North America and the former Soviet Union. It should be noted, however, that there is much year-to-year variability in snowpack characteristics and that both snowfall and the processes causing metamorphism occur at highly variable rates over short distances, due largely to differences in slope, aspect, and vegetative cover.

At the beginning of the melt season, the snowpack is typically vertically heterogeneous as well, with perhaps several layers of markedly contrasting densities. During melt, density continues to increase and the vertical inhomogeneities tend to disappear. During this period, density can fluctuate on an hourly or daily time scale due to the formation and drainage of melt water. Snowpacks that are at 0 °C and well drained tend to have relative densities near 0.35 (McKay 1970).

5.2 MEASUREMENT OF SNOW AND SNOWMELT

Discussion of measurement of snow and snowmelt requires definition of several terms:

Precipitation is the depth of rainfall plus the water equivalent of snow, sleet, and hail falling during a given storm or measurement period.

Snowfall is the incremental depth of snow and other forms of solid precipitation that accumu-

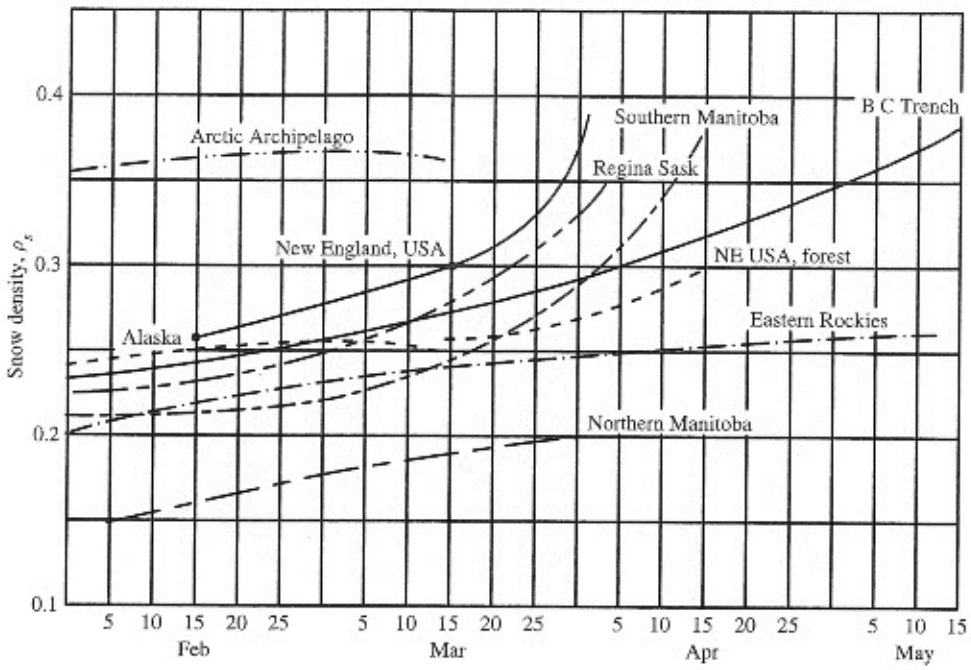

FIGURE 5-2
Seasonal variation in snowpack relative densities in various regions of North America. Modified from McKay (1970).

lates on the surface during a given storm event or measurement period.

Snowpack refers to the accumulated snow on the ground at a time of measurement. The snowpack water equivalent and areal extent are of particular hydrologic importance; information on depth and density is also useful.

Snowmelt is the amount of liquid water produced by melting that leaves the snowpack during a given time period; it is usually expressed as a depth.

Ablation is the total loss of water substance (snowmelt plus evaporation/sublimation) from the snowpack during a given time period; it is usually expressed as a depth.

Water output is the total amount (depth) of liquid water (rain plus snowmelt) leaving the snowpack during a given time period.

Snow drifting during storms can produce large variations in snow depth and density over short distances, and variations in subsequent snow metamorphism, melting, and evaporation due to local wind, temperature, radiation, and other microclimatic conditions can further modify the distribution of these properties. Thus snow characteristics will be highly variable in space, mainly because of variations in vegetative cover, slope, and aspect (slope orientation); consequently, obtaining a representative picture of the distribution of snow and snow properties is important and usually difficult. Remotely-sensed information that simply shows areas with and without snowcover within the region of interest can be extremely valuable in assessing the amount of water present in the form of snow. Peck (1997) has emphasized that particular care must be taken in obtaining reliable hydrometeorological measurements in cold regions and has stressed that a smaller number of high-quality records may be more valuable than a larger number of records of questionable quality.

Approaches to measurement of each of the quantities listed previously are discussed next and summarized in Table 5-1.

5.2.1 Precipitation

Standard Gages

As discussed in Section 4.2.1, precipitation is measured by collecting gages in which the snow and ice have melted or that weigh the total in-falling water

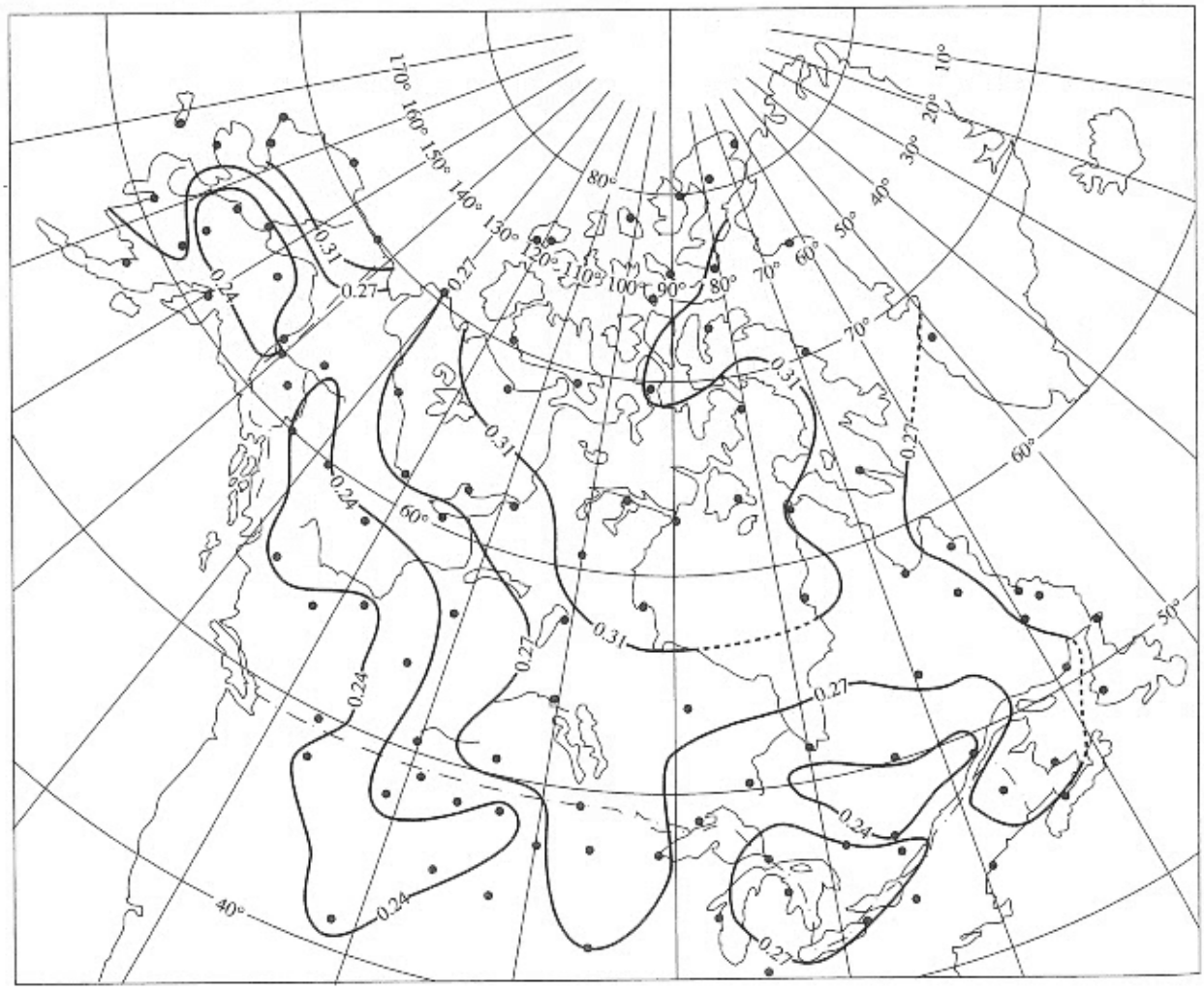

FIGURE 5-3
Average seasonal snowpack relative densities (ρ_s/ρ_w) for North America. From Bilello (1984).

substance. In most cases, the form of the precipitation is not recorded.

We have seen that measurements in such gages are subject to several sources of error, the most important of which is due to wind. Most network precipitation gages in the United States lack windshields, and even those equipped with Alter-type shields suffer from generally significant catch deficiencies for snow [Figure 4-16; Equations (4-3)]. Studies in Canada indicate that a specially designed gage with a Nipher windshield (Figure 5-5) maintains an adequate gage catch in winds up to about 5.5 m s^{-1}, but as of 1980 only 14% of Canadian gages were equipped with such shields (Goodison et al. 1981). Gages used in the former Soviet Union and most other northern countries also suffer from wind-induced catch deficiencies, so that standard network measurements must be assessed with caution for periods in which snow is an important component of precipitation (Legates and DeLiberty 1993; Yang et al. 1998).

Universal Gage

Cox (1971) developed a "universal surface precipitation gage" that measures snowfall and snowpack water equivalent by weight and collects and measures water output, so that all of the quantities

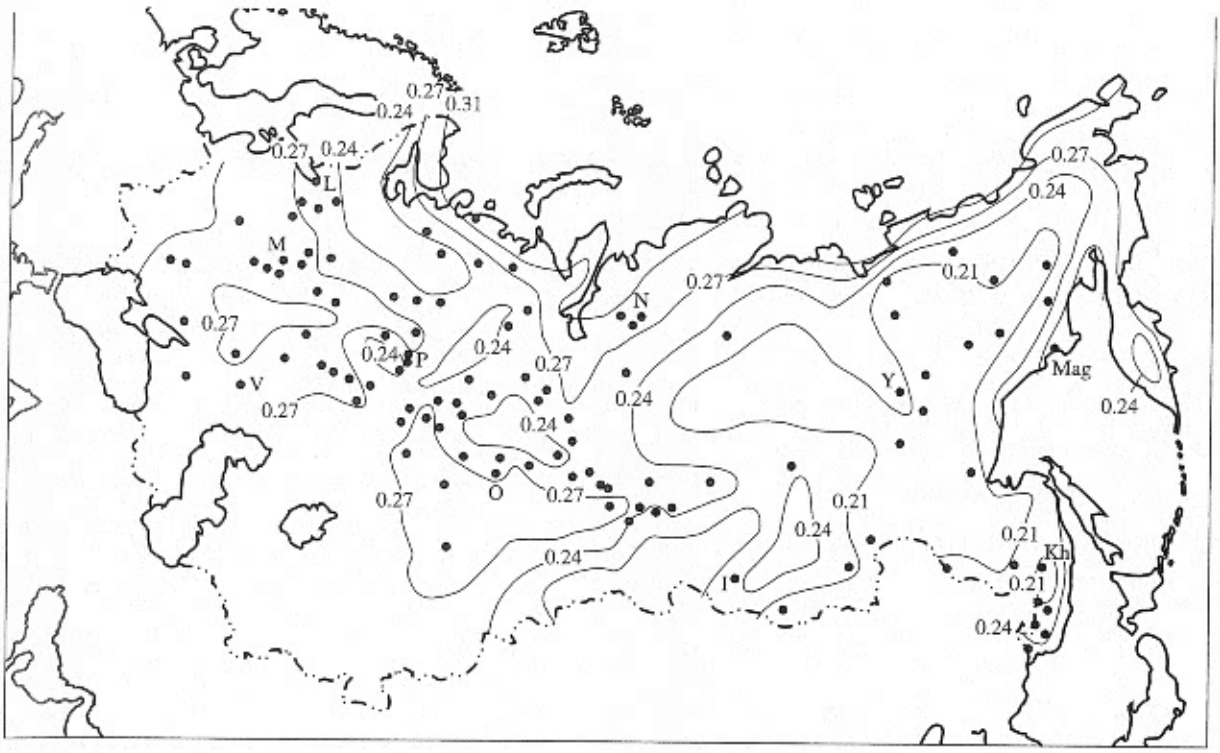

FIGURE 5-4
Average seasonal snowpack relative densities (ρ_s/ρ_w) for the former Soviet Union. From Bilello (1984).

TABLE 5-1
Methods of Measuring Depth, Water Equivalent, and Areal Extent of Precipitation, Snowfall, Snowpack and Snowmelt-Water Output. Letters in parentheses indicate ground based (G), aircraft based (A), satellite based (S).

Parameter	Depth	Water Equivalent	Areal Extent
Precipitation	—	Standard storage gages (G) Universal gage (G)	Gage networks (G) Radar (G)
Snowfall	Ruler, board (G)	Melt snow on board (G) Use estimated density (G) Universal gage (G) Snow pillow (G)	Observation networks (G) Radar (G) Visible/Infrared (S)
Snowpack	Snow stake (G,A) Snow tube (G) Acoustic gage (G)	Universal gage (G) Snow tube (G) Snow pillow (G) Artificial radioisotope gage (G) Natural gamma radiation (G,A) Microwave/radar (A,S)	Snow surveys (G) Visible/Infrared (S) Microwave/radar (A,S) Snow-pillow network (G)
Snowmelt and Water Output		Snow pillow (G) Lysimeter (G) Universal gage (G)	

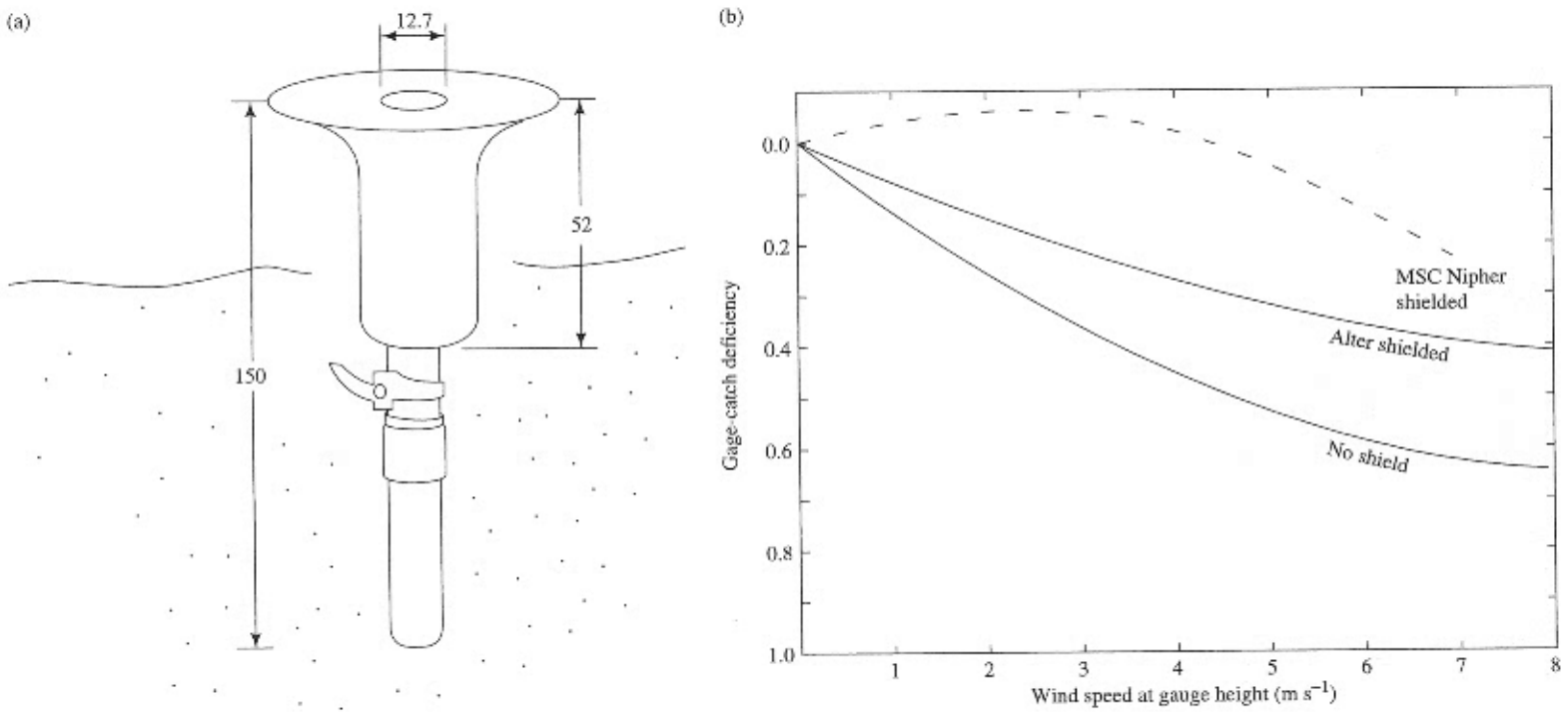

FIGURE 5-5
Canadian precipitation gage with Nipher windshield for areas with significant snowfall. (a) Dimensions of gage (cm). The gage is adjusted so that its orifice is maintained at 150 cm above the snow surface. (b) Comparison of gage-catch deficiency for snow as a function of wind speed for Canadian Nipher shield, Alter shield, and no shield. Data from Goodison et al. (1981) and Larson and Peck (1974).

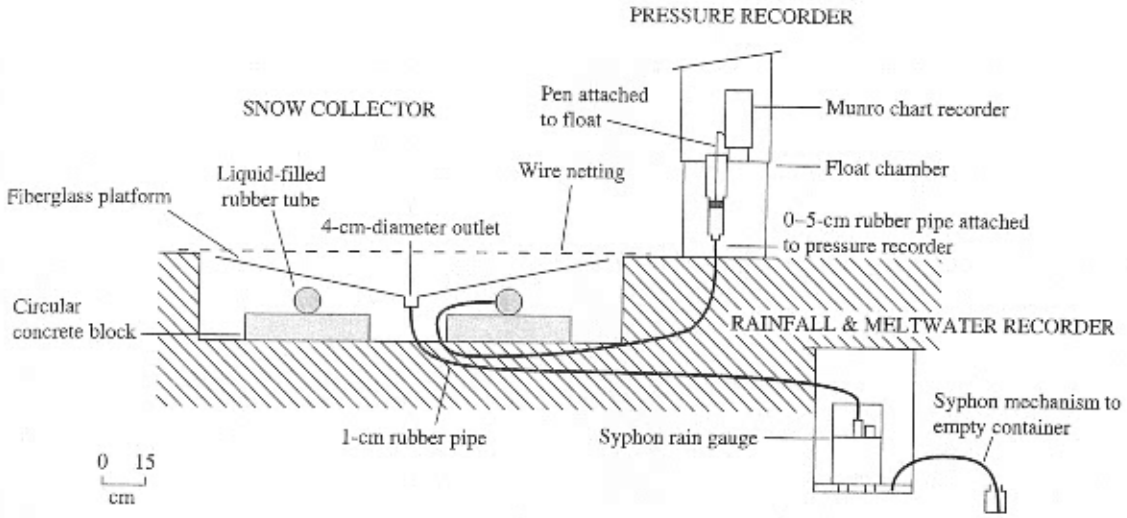

FIGURE 5-6
Diagram of the universal gage, which can measure precipitation, snowfall, water equivalent, and water output. From Waring and Jones (1980).

listed in Table 5-1 are simultaneously determined and recorded. Waring and Jones (1980) modified Cox's design to make it more suitable for shallow snowpacks (Figure 5-6). Clearly, these gages are considerably more elaborate and expensive to install than are standard gages, and they are therefore not widely used in observation networks.

Radar

As described in Section 4.3.5, radar observations can be used to determine the areal extent and type of precipitation and to provide general information on precipitation rates.

5.2.2 Snowfall

Standard Methods

Snowfall depth is usually measured simply by placing a ruler vertically on a board that had been set on the surface of the previous snowpack. The water equivalent of snowfall can be determined by melting the snow collected on the board and measuring its volume, although it is more common simply to estimate this value by assuming a density, usually 100 kg m^{-3}.

Universal Gage

The universal gage (Figure 5-6) measures snowfall water equivalent by recording an increase in weight on the collector in the absence of near-simultaneous production of water output. Similarly, an increase in the weight recorded by a snow pillow (see later) would usually indicate a snowfall event, although rainfall that stayed in the snowpack would also cause a weight increase.

Radar

Snowflakes reflect radar waves more strongly than do raindrops, so radar images can distinguish between the two forms of precipitation and can be used to delineate the areal extent of snowfall for a given storm. However, radar measurement of snowfall rates is even more difficult than of rainfall rates, because the various forms of snowflakes have greatly differing radar reflectivities (Goodison et al. 1981).

5.2.3 Snowpack

Snow Stakes

The depth of snow can be observed simply by inserting a ruler or similar device through the snow to

the ground surface, or by observing the height of the snow surface against a fixed ruler, called a **snow stake,** with its zero point at the ground surface. In some remote areas, permanent snow stakes are designed with large markings so that readings can be made from aircraft.

Snow Surveys

The most important snow information for the hydrologist is the water equivalent of the snowpack. Network measurements of this quantity are most commonly obtained via periodic **snow surveys** at fixed locations, called **snow courses.** A snow course is a path between two fixed end points over which a series of measurements of snow depth and water equivalent are made. The length of the path is typically 150 to 250 m, with measurements made at about six points (more if snow conditions are highly variable) spaced at a fixed interval of at least 30 m. At each point, a coring tube equipped with a toothed cutting rim, called a **snow tube** (Figure 5-7), is inserted vertically to the surface. After the snow depth is read against markings on the outside of the tube, the tube is pushed a few centimeters into the soil and twisted to secure a small plug of soil that retains the snow in the tube. The tube is then extracted and weighed on a specially calibrated scale that is pre-tared and reads directly in centimeters or inches of water equivalent. Density at each point can be calculated via Equation (5-12), and water equivalent for the course is the average of the values at the measurement points.

EXAMPLE 5-1

Snow surveyors measured the snowpack depths and water equivalents given in the accompanying table using a snow tube at five points along a snow course in the Kootenai River Basin, Montana, on 27 February 1958. Compute the average depth, water equivalent, and density for this location.

Point	1	2	3	4	5
Depth (cm)	98	108	102	109	105
Water Equiv. (cm)	27	30	27	30	29

Solution The average depth and the water equivalent are found simply as the arithmetic averages of the five observations: 104 cm and 29 cm, respectively. The density at each point is found via Equation (5-12), with $\rho_w = 1000$ kg m^{-3}:

Point	1	2	3	4	5
Density (kg m^{-3})	280	280	260	280	280

Thus, the average density is 280 kg m^{-3}.

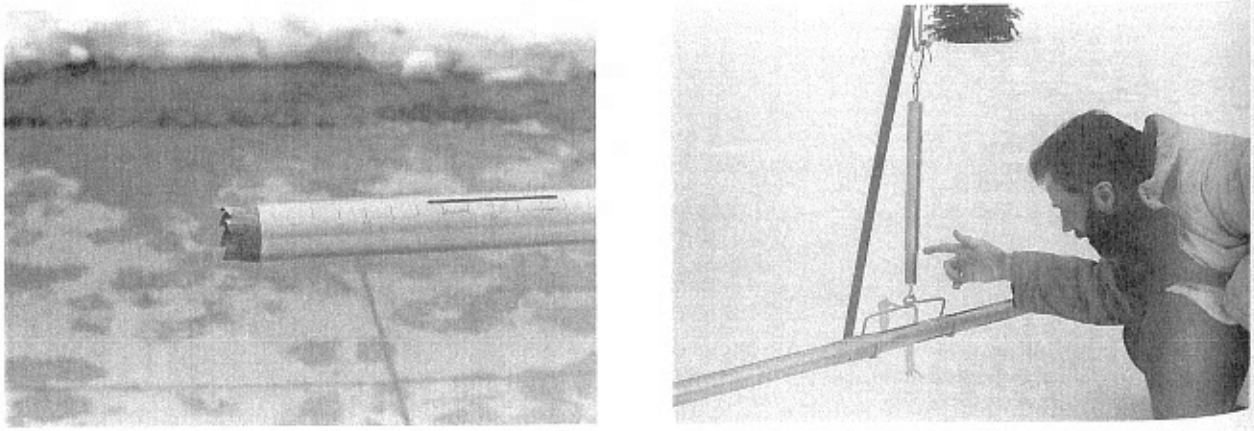

(a) (b)

FIGURE 5-7
(a) Snow tube showing cutter. (b) Determining water equivalent with a snow tube. Photo by author.

Several different designs of snow tubes are available; the tubes may be made of aluminum or fiberglass and range in diameter from 3.8 to 7.6 cm. Comparisons of measurements taken by snow tubes with measurements taken by carefully excavating and weighing snow have shown that most snow tubes tend to overestimate water equivalent by up to 10% (Work et al. 1965; Goodison et al. 1981).

In shallow (i.e., less than about 1 m) snowpacks, depth and density have been found to be essentially independent, and there is typically less temporal and spatial variability in density than in depth (Goodison et al. 1981); this is clearly the case in Example 5-1. Under these conditions, little precision is lost and considerable time may be gained by making more depth measurements than water-equivalent measurements. Rikhter (1954) suggested a rough field guide to variations in density: Snow with a relative density of 0.32 to 0.35 will support an adult without skis; at 0.35 to 0.38, an adult's foot leaves only a slight impression; and above 0.4, the foot leaves no mark on the surface.

A snow-course network, like a precipitation-gage network, should be designed to provide a representative picture of the snowpack in the region of interest. However, since measurements are labor intensive, snow courses are usually considerably more widely spaced than gages and are usually read at longer time intervals—e.g., every two weeks during the snow season. Because snowpack conditions are largely determined by local conditions, it is usually sound strategy to design the network to sample representative ranges of land use (vegetative cover), slope, aspect, and elevation. Areal averages may then be estimated by extrapolating from these measurements on the basis of the distribution of the various conditions in the region of interest. However, for operational purposes such as forecasting runoff, measurement agencies commonly rely on only a few snow-course sites that have been "calibrated" over a period of years to provide an index, rather than a sample estimate, of the watershed snowcover.

Snow Pillows

The water equivalent of snowpack can also be measured with **snow pillows,** which are circular or octagonal membranes made of rubber or flexible metal that contain a liquid with a low freezing point (Figure 5-8). The weight of the snow on the pillow controls the pressure of the liquid, which is recorded or monitored via a manometer or pressure transducer.

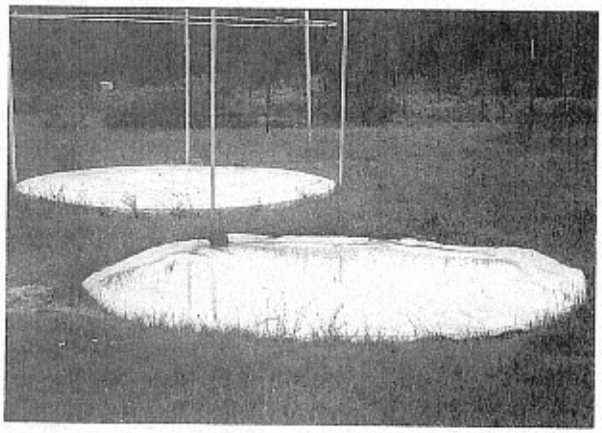

FIGURE 5-8
A snow pillow (foreground) and a water-output lysimeter (background) installed at the U.S. National Weather snow-research site at Danville, VT. Buried lines transmit the fluid pressure from the pillow to a sensor, and the water released by the snowpack to a measuring device, both of which are in an instrument shelter. The metal ring is electrically heated and is melted down through the snowpack to isolate the cylinder of snow above the lysimeter. Photo by author.

The diameter of snow pillows ranges from 1 to 4 m, with larger diameters recommended for deeper snowpacks (Barton 1974). Several factors influence the accuracy and continuity of readings, including (1) leaks; (2) temperature variations that affect the density of the liquid; (3) the formation of ice layers within the snowpack, which can support a portion of the snow and lead to undermeasurement of water equivalent (called "bridging"); (4) disruption of the contact between the snow and the ground, which can distort the snowpack energy and water balances; and, in remote installations, (5) instability of power supply to sensors and recorders. Detailed considerations for installation and maintenance of snow pillows were given by Davis (1973) and Cox et al. (1978), and measurement problems were discussed by McGurk and Azuma (1992) and McGurk et al. (1993).

Snow pillows are well suited for remote installation, with pressure readings transmitted by telemetry. In Alaska and the 12 western states of

the U.S. mainland, the U.S. Natural Resources Conservation Service (NRCS) operates the SNOTEL network of 560 snow pillows, which provides telemetered data on water equivalent with an accuracy of about 2.5 mm (Schaefer and Werner 1966). If read frequently enough, snow pillows can be used to measure the water equivalent of individual snowfalls.

The universal gage (Figure 5-6) measures snowpack water equivalent using the same basic principle as that of the snow pillow.

Acoustic Gages

Chow (1992) described a system that measures snow depth ultrasonically. The system is commercially available at relatively low cost and is well suited for installation as part of an automatic weather station.

Radioactive Gages

Several types of instruments exploiting the attenuation of gamma rays or neutrons by water substance can be used for nondestructive measurement of the water equivalent of the snowpack. One version involves an artificial gamma-ray source (^{60}Co or ^{137}Cs) and a detector, one of which is at the ground surface and the other suspended above the ground; the readings from the detector are typically transmitted by telemetry from a remote location to the observer. Bland et al. (1997) reported a method by which a portable gamma-ray source is inserted into permanent structures in the field at the time of measurement, and a hand-held detector is used to make a nondestructive determination of water equivalent with a precision of 3 mm.

For snowpacks with water equivalents less than about 40 cm, it is also possible to measure the attenuation by snow of natural gamma radiation emitted from the soil surface using a detector either fixed a few meters above the surface (Bissell and Peck 1973) or mounted on an aircraft (Loijens and Grasty 1973). Use of an airborne detector requires low-altitude (< 150 m) flights along a route over which the snow-free gamma emission has been previously determined; corrections must then be made to account for soil moisture and radioactive emissions from the air (Goodison et al. 1981; Foster et al. 1987). However, work by Grasty (1979) suggested that a simpler, single-flight technique can give results of high accuracy. Carroll and Voss (1984) found good correlation between water equivalents determined from airborne gamma-radiation sensors and snow tubes in forested regions of the northern United States and of Canada (Figure 5-9a), as did Bergstrom and Brandt (1985) in Sweden. The U.S. National Weather Service now routinely uses low-flying aircraft to estimate water equivalents from natural gamma radiation (Carroll and Carroll 1989).

Airborne Microwave and Radar

Microwave radiation (wavelengths of 0.1 to 50 cm), including radar, can be used to remotely measure the water equivalent, areal extent, and other properties of the snowpack. Airborne systems exploiting these wavelengths have the advantage of being able to "see through" clouds; however, many variables affect the observations, and methods for interpreting data are still being worked out.

The flux of microwave radiation emitted by a snowpack depends on its temperature, grain size, and the underlying soil conditions, as well as on its density. Thus considerable information about ground conditions is required for translating "passive" microwave emissions to estimates of water equivalent, and research is currently underway to provide reliable algorithms for interpretation (Foster et al. 1987).

Radar observation involves directing a beam of microwave radiation at the snowpack and measuring the strength of the reflected energy. This radiation can penetrate into the pack, so it can be used to provide information about snowpack stratigraphy and liquid-water content, as well as water equivalent, if sufficient information about surface cover and topography is available.

Satellites

Satellite imagery using visible, infrared, and microwave wavelengths provides information on the areal extent of snow cover for large areas. Although careful interpretation is required to distinguish snow from clouds and to identify snow in areas of forest and highly reflective land surfaces, the most accurate maps of areal snow cover to date have been produced from visible-wavelength images. These images have been the basis for weekly maps that have been produced since 1978 for northern-hemisphere land, with a resolution of about 1.2 km^2 (Robinson et al. 1993).

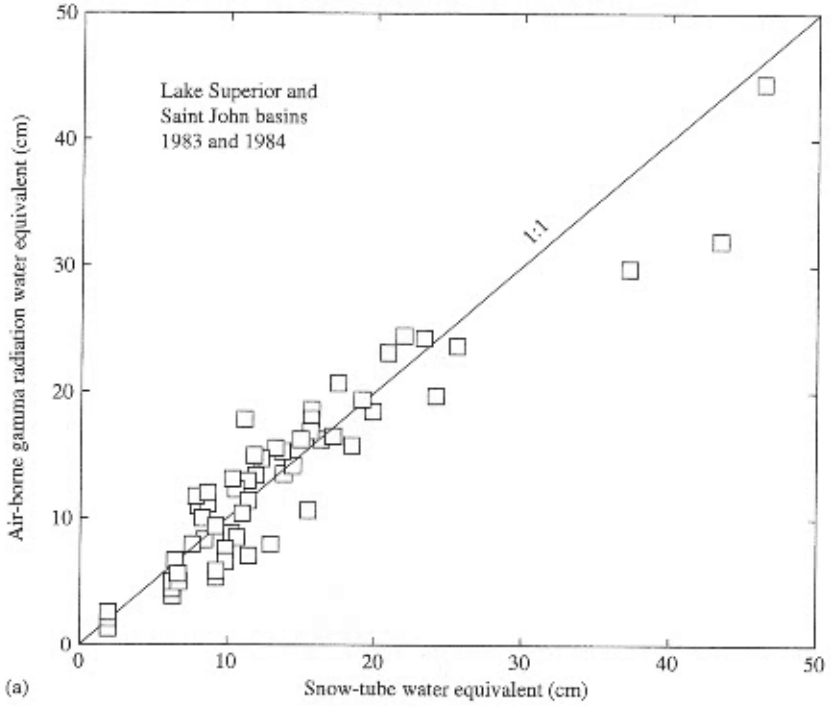

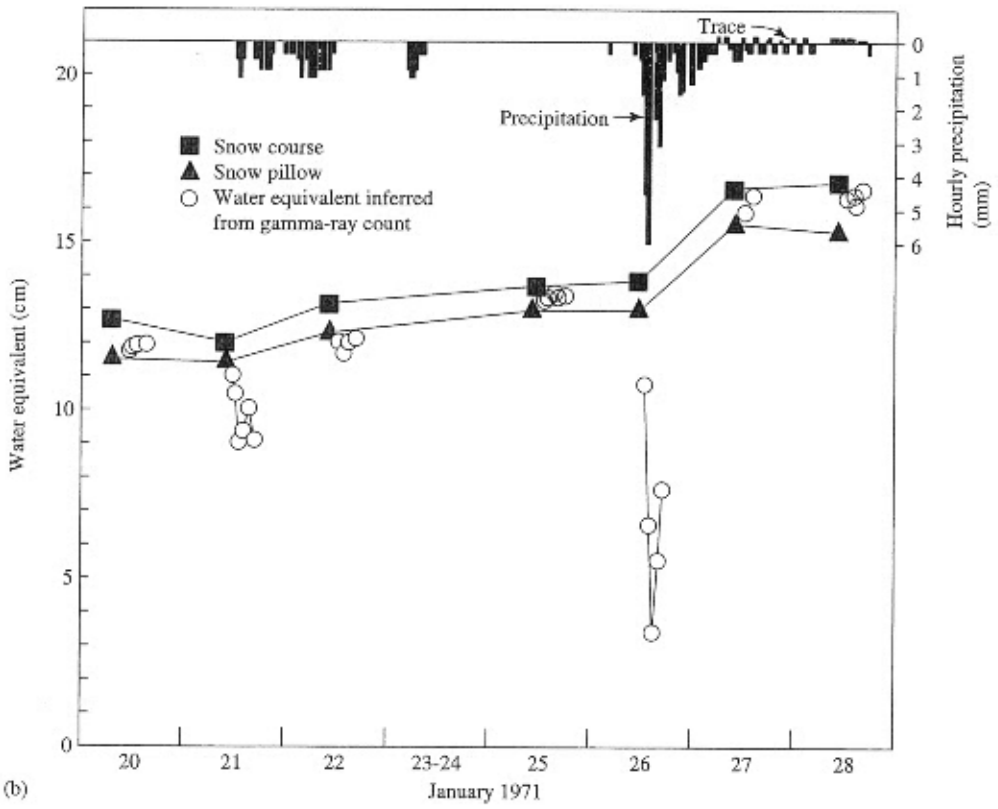

FIGURE 5-9
(a) Comparison of water equivalent determined by airborne gamma-radiation sensors and snow-tube measurements in the Lake Superior and St. John River Basins, United States and Canada. From Carroll and Voss (1984). (b) Water equivalent of snowpack at Danville, VT, measured over nine days by snow tube, snow pillow, and attenuation of natural gamma radiation. The false low readings of the radiation detector were due to radioactivity deposited during snowstorms and could easily be corrected for. From Bissell and Peck (1973); used with permission of the American Geophysical Union.

More recently, algorithms have been developed for mapping the distribution of snow cover over wide areas by automated analysis of satellite-borne radiometer data. These algorithms use reflected and emitted energy in several visible and infrared wavelengths to differentiate between clouds and snow and to correctly interpret variations produced by forest cover and shading. Rosenthal and Dozier (1996) described an algorithm for mapping mountain snow-cover extent from the Landsat Thematic Mapper satellite, which has a resolution of about 800 m^2. A new methodology for automated analysis of visible and infrared radiation collected by the AVHRR (Advanced Very High Resolution Radiometer) satellite can separate clouds from snow and clear land under most conditions, and the results can be used to produce daily continental-scale maps of the areal extent of snow cover with a resolution of 1.1 km^2 and 97% accuracy (Simpson et al. 1998).

Overview

In spite of their slight tendency to over measure, snow-survey observations are usually considered the most accurate "routine" measurements of water equivalent. However, they are labor intensive and impractical for routine use in remote areas. Snow pillows are accurate and are widely used in the western United States for remote monitoring of mountain snowpacks; however, they are subject to bridging, temperature effects, and failures of instrument components (Goodison et al. 1981; McGurk et al. 1993).

Figure 5-9b compares water equivalents measured via snow tube, snow pillow, and a fixed radioisotope gage over several days at one location. Natural radioactivity deposited with falling snow caused false low readings by the gamma detector, but this radioactivity was found to decay rapidly and could readily be corrected for (Bissell and Peck 1973). Thus, all three methods appear to give similar results.

Goodison (1981) compared snow-survey and snowfall data in Canada and found that compatible estimates of regional water equivalents were possible only if (1) snow-survey data are weighted to account for the variability of water equivalent as a function of land use and (2) precipitation-gage measurements of snowfall are corrected for gage-catch deficiencies due to wind.

Remotely-sensed observations via aircraft or satellite using active or passive microwave, infrared, or visible wavelengths are becoming increasingly relied on for information on the areal extent of snow cover. Maps of snow-cover extent in the northern hemisphere derived from satellite observations, beginning in 1978, are available from the U.S. National Oceanic and Atmospheric Administration (NOAA) as the NOAA-NESDIS Weekly Northern Hemisphere Snow Charts, and similar maps based on newer satellite sensors and interpretation algorithms are becoming available. Such observations of the areal extent of snow cover, along with water-equivalent information developed from telemetered remote snow pillows and airborne detection of gamma radiation, are widely used for water-resource management decisions, especially in the western United States.

Techniques involving spatial correlation, similar to those described for mapping of areal precipitation (Box 4-2), have been developed and are routinely used for mapping the areal distribution of water equivalent in the United States (Carroll and Cressie 1996).

5.2.4 Snowmelt, Ablation, and Water Output

Lysimeters

The most straightforward method for measuring water output is via a **lysimeter** (Figure 5-8), which collects the water draining from the overlying snow and directs it to a device that measures and records the flow. This instrument may be fitted with a circular metal ring that can be electrically heated and lowered through the snow to isolate the cylinder of snow above the collecting surface; this method avoids gaining or losing water that might be moving horizontally along ice layers in the snowpack.

Note that, as with snow pillows, snow conditions above a lysimeter may differ from those in the natural snowpack due to interruption of the snow–ground connection.

Snow Pillows

Snow pillows detect ablation as a decrease in weight (assuming the water runs off the pillow); in many cases, evaporation can be considered negligible and the weight change can be attributed to water output.

Universal Gage

As noted previously, universal gages collect and measure water output. Water output occurring at the same time as a corresponding weight decrease indicates snowmelt; water output in the absence of a weight decrease indicates rainfall; and a weight decrease in the absence of water output indicates evaporation.

Pans

Specific measurement of evaporation and sublimation of the snowpack can be made using pans that are periodically weighed. Slaughter (1966) reviewed studies that employed various types of pans and concluded that good measurements can be obtained using pans that are made of plastic or metal, as long as the edge of the pan is flush with the snow surface and the surface roughness of the snow in the pan is the same as that of the surrounding snowpack. The pan should be at least 10 cm deep to avoid absorption of radiation by the bottom of the pan and, if significant melt is occurring, should be designed to allow meltwater to drain into a collector for separate measurement.

5.3 HYDROLOGIC IMPORTANCE AND DISTRIBUTION OF SNOW

5.3.1 Water Input

Precipitation in the form of snow is usually stored for a significant period on the ground surface and does not become an input to the land phase of the hydrologic cycle until it melts. Thus it is hydrologically useful to define **water input** as the sum of rainfall plus snowmelt for a given time period. When a snowpack is present, water input equals the water output from the snowpack.

In areas with a seasonal snowpack, the amount and timing of **surplus water input** (water input minus evapotranspiration), rather than of **surplus precipitation** (precipitation minus evapotranspiration), largely determines the amount and timing of streamflow and ground-water recharge (Figure 5-10). However, in spite of the strong relationship between water-input climate and hydrologic climate, there have been few studies characterizing water-input climatology. Hendrick and DeAngelis (1976) showed that water-input climatology in New England is determined by latitude and elevation; they developed a method for determining climatic and synoptic patterns of water input from standard network observations of temperature and precipitation. Further research along these lines would clearly be useful for many hydrologic purposes, including predicting the effects of climate change on streamflow.

5.3.2 Distribution of Snow

Global

Virtually all the land above 40° N latitude has a seasonal snow cover of significant duration (Figure 3-21); this amounts to about 42% of the land in the northern hemisphere. Figure 5-11 shows the steep latitudinal increase in the fraction of average annual precipitation falling as snow in North America; this fraction reaches about 0.65 on the north coast of Alaska (Dingman et al. 1980). Location relative to oceans and elevation also influences the portion of precipitation occurring as snow.

Average dates of formation and disappearance of snow cover are shown in Figure 5-12 for North America and in Figure 5-13 for the former Soviet Union. Figure 5-14 gives average seasonal maximum snow depths in the northern hemisphere. As noted earlier, maps and statistics of weekly northern hemisphere snow-cover extent since 1978 are available and show that snow cover has been declining over the last two decades (Robinson et al. 1993; Box 3-3).

Because of the lack of detailed knowledge of runoff processes (Chapter 9), it is difficult to quantify the fraction of runoff derived from snowmelt. However, a smaller proportion of snowfall than of rainfall is evaporated and transpired, so it is clear that snowfall contributes proportionally more to runoff. L'vovich (1974) estimated that more than half the annual runoff is derived from snowmelt in much of the northern hemisphere (Figure 5-15).

Elevational

Because of the general decrease of air temperature with altitude (Figure D-2), the fraction of precipitation falling as snow, and the water equivalent of

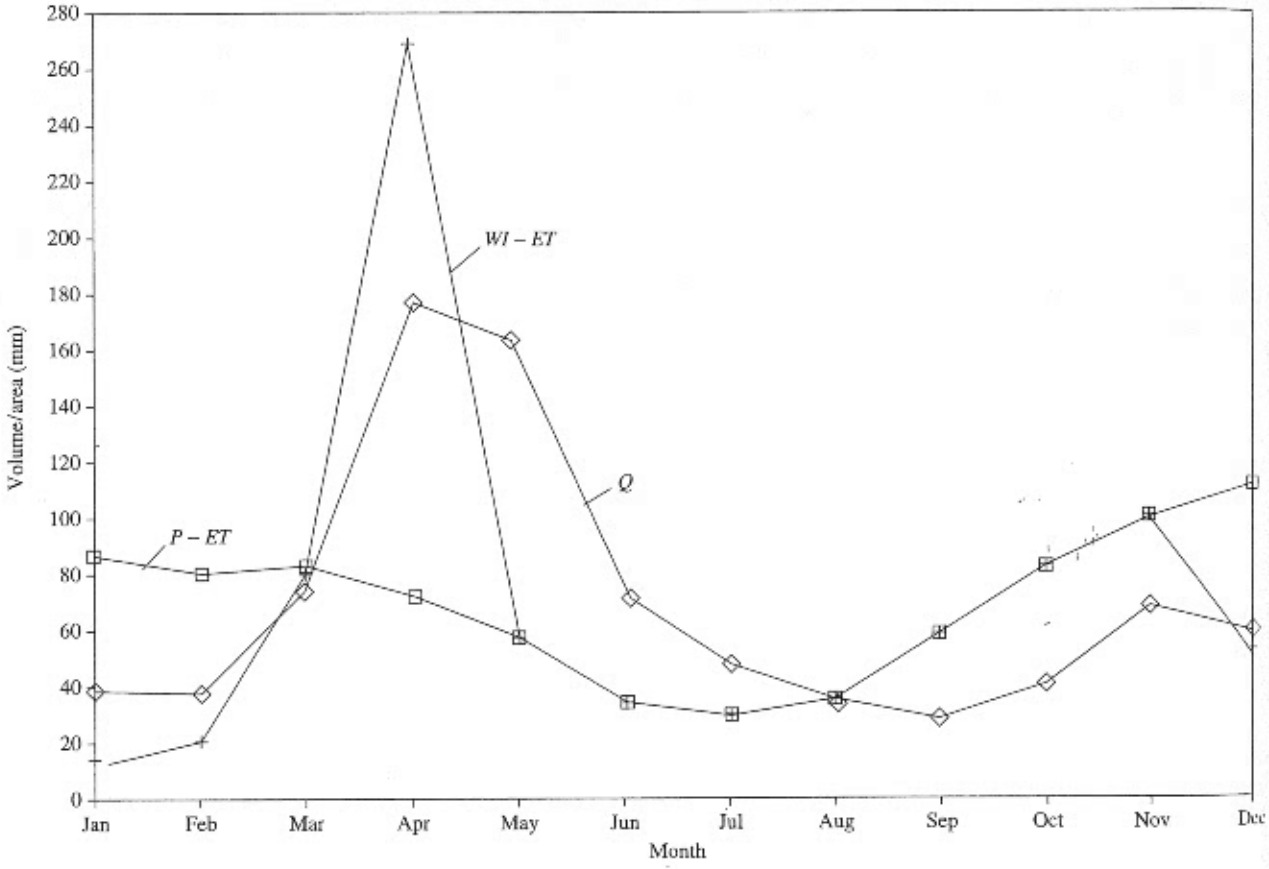

FIGURE 5-10
Average monthly precipitation minus evapotranspiration ($P - ET$) and water input minus evapotranspiration ($WI - ET$) compared with streamflow (Q) in the Pemigewasset River basin, NH. The timing of streamflow is more closely related to $WI - ET$ than to $P - ET$.

snow, are usually strong functions of elevation in a region (Figure 5-16). For mountain regions, as much as 85% of the annual runoff may come from snowmelt (Shafer and Dezman 1982).

Rates of increase of water equivalent with elevation vary regionally and with local factors such as aspect (i.e., north- or south-facing slopes) and vary from year to year at a given location. Meiman (1968) reviewed a number of studies on the elevational distribution of snow in North America and reported rates of increase of water equivalent ranging from 5.8 to 220 mm per 100 m elevation. Caine (1975) found that the year-to-year variability of water equivalent decreased with elevation in the southern Rocky Mountains, USA.

Local

As noted in Section 5.2, snow properties are highly dependent on local site factors such as aspect (slope orientation) and vegetation cover. In general, local variability will be greatest in regions where periods of melting occur during the winter, where there are pronounced spatial changes in land cover and topography, and where much of the heat input to the snow is from solar radiation.

The main effect of aspect is on energy inputs from solar radiation, resulting in faster densification and melting on south-facing slopes. Aspect may also affect the wind microclimate, which in turn affects snow deposition and densification and energy exchanges of sensible and latent heats. These en-

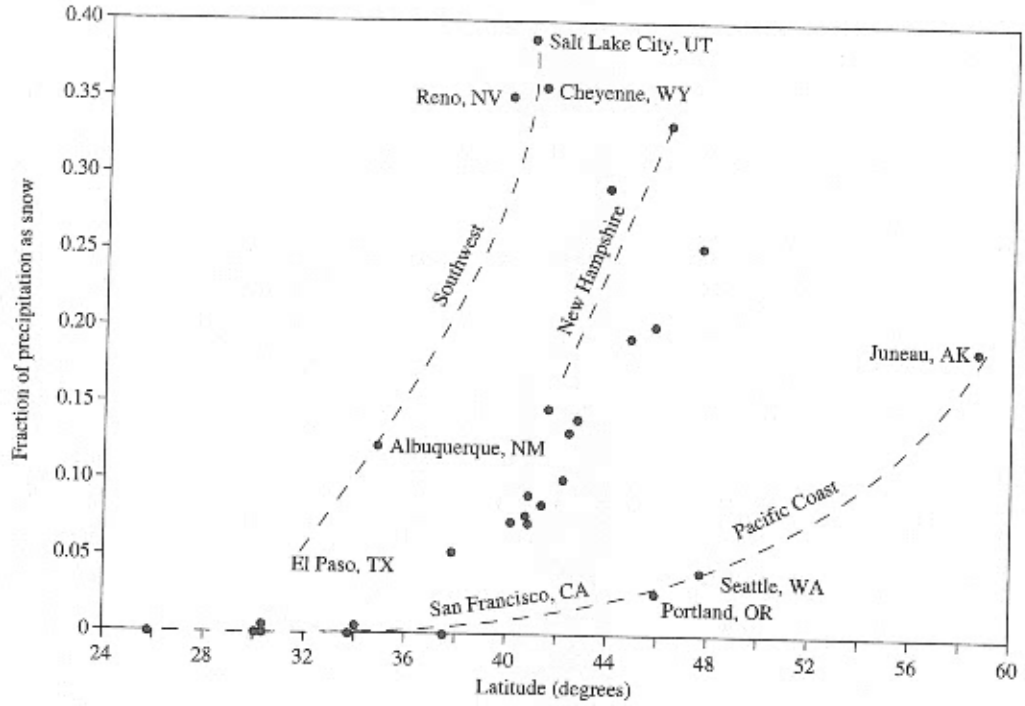

FIGURE 5-11
Fraction of precipitation occurring as snow as a function of latitude in the United States. City data from Todd (1970); unidentified points are for cities east of the Rocky Mountains.

ergy exchanges are discussed quantitatively in Section 5.4.

The accumulation of precipitation on the leaves and branches of vegetation is called **canopy interception.** Some intercepted snow eventually falls to the ground either before or after melting and is added to the snowpack; the rest evaporates and is called **canopy interception loss.**[1] Clearly, deciduous trees intercept less snow than do conifers, and various conifer species differ in their capture of snow. Schmidt and Gluns (1991) found that (1) individual conifer branches intercepted 11 to 80% of snow (water equivalent) in 22 storms, (2) the fraction intercepted was inversely related to snow density (ρ_s/ρ_w) and to total storm precipitation, and (3) the maximum intercepted water equivalent was about 7 mm. Thus in forests a large proportion of snowfall is intercepted, but most studies have found that it is of minor hydrologic importance (Hoover 1971; Tennyson et al. 1974), because most intercepted snow falls to the ground or melts rather than evaporates.

Forest clearings and thinnings disrupt the typical upward-increasing wind velocities above a canopy (see Section D.6.3) and generally lead to increased snow deposition. Many studies have shown that snow accumulation is greater in small (i.e., diameters less than $20 \cdot z_f$, where z_f is the height of surrounding trees) forest clearings than in the surrounding forest. The relative importance of wind redistribution and interception in producing these differences changes from region to region. However, for clearings larger than $20 \cdot z_f$, the accumulation pattern tends to be reversed, because the wind speed tends to be higher than in the forest; this redistributes snow into the surrounding forest and causes higher evaporation in the clearing (Golding and Swanson 1986).

Watershed-scale experiments have shown that both selective and clear-cutting tree harvesting tend to increase snowpack water equivalent and snowmelt runoff (Schmidt and Troendle 1989). This

[1] Rainfall interception and interception loss are discussed in detail in Section 7.6.

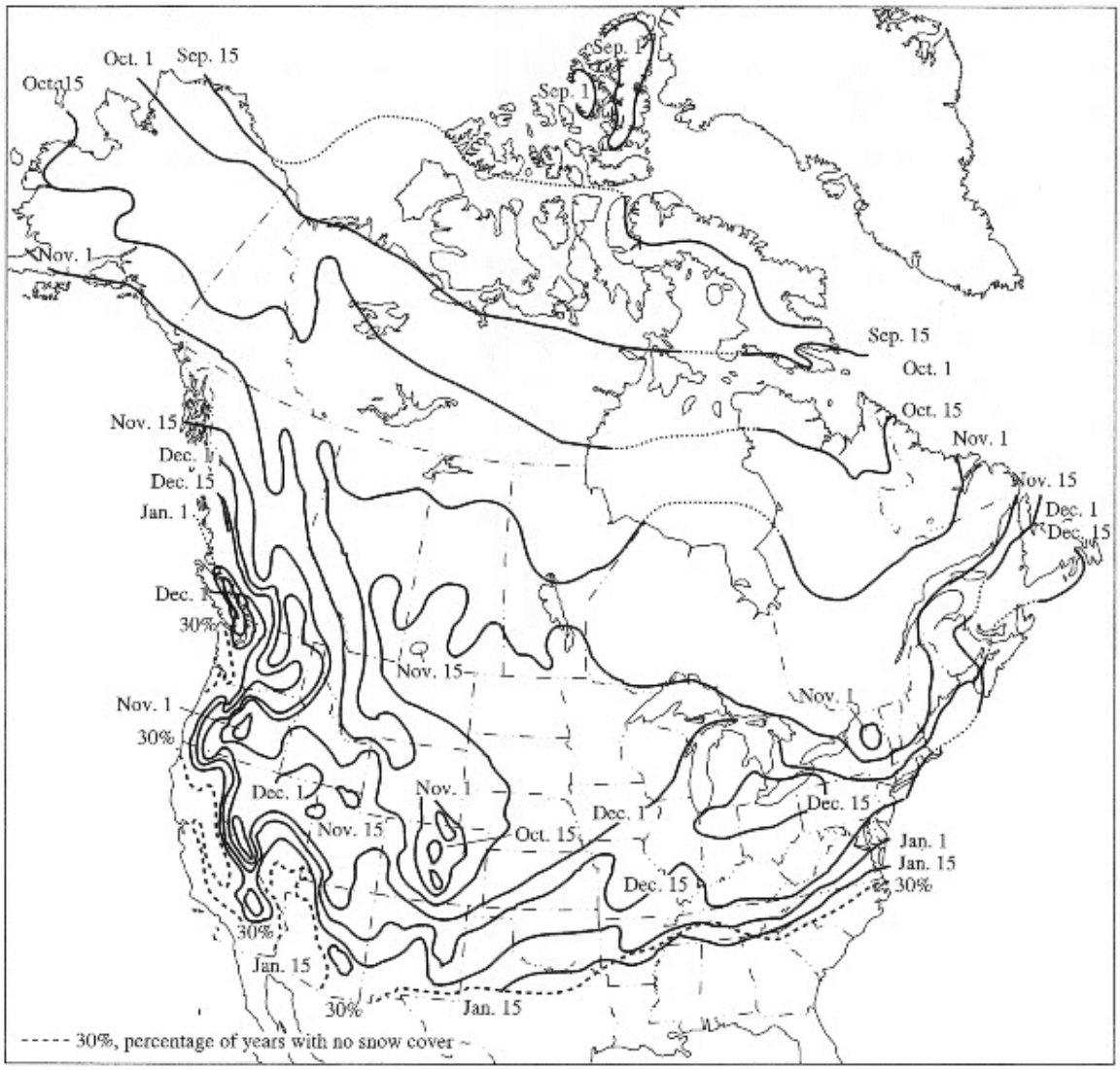

(a)

FIGURE 5-12
Average date of snow cover (a) formation and (b) disappearance in North America. From McKay and Gray (1981).

increase is attributed to a reduction in the evaporation of intercepted snow and increased snow deposition into clearings and thinned forests, partially offset by increased evaporation from the ground snowpack.

Figure 5-17 shows the variability of seasonal peak depth, density, and water equivalent on a range of vegetation types in Ontario, Canada. Overall, these observations are consistent with those just described for forest clearings: The highest depths and water equivalents were in an open forest with shrub understory (Vegetation Zone B), and the lowest values were in areas without forest cover, including grass (Zone A) and marsh (Adams 1976). Density tended to vary little with land-cover type. Note also that there was considerable year-to-year variability in the relative values.

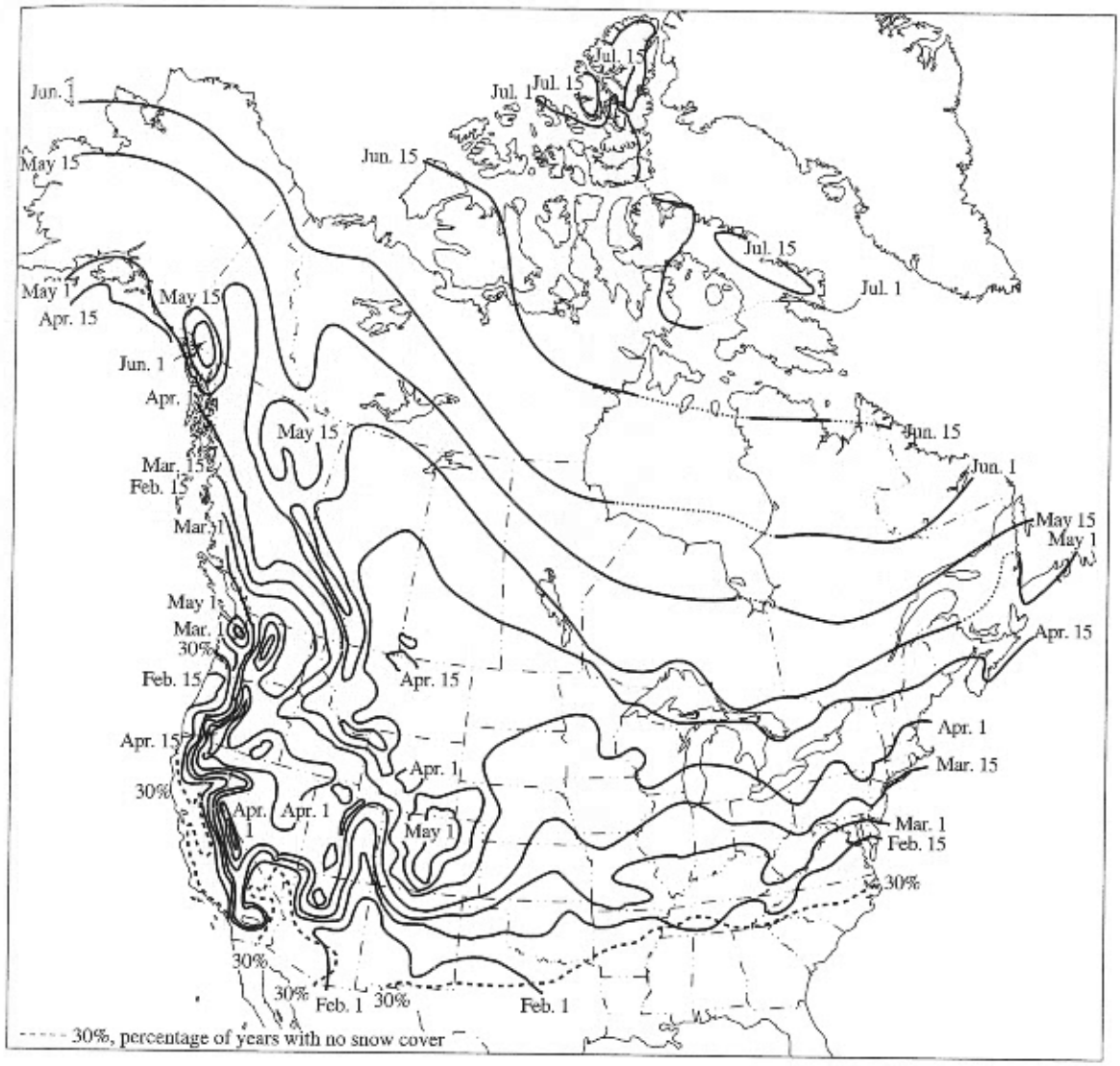

(b)

FIGURE 5-12
Continued

On an even more local scale, Woo and Steer (1986) presented data on variations of snow depth around individual trees in a subarctic spruce forest in northern Ontario. The data were used, along with information on tree spacing, to compute the average snow depth for the forest. As shown in Figure 5-18, depth increases nonlinearly away from the trunk and reaches the clearing value at a distance of 2 to 4 m from the tree. Presumably, this pattern is produced by snow interception and by added heat inputs due to longwave radiation from the tree trunk, which can accelerate the processes that increase snow density and produce melt.

Donald et al. (1995) developed relations between land-cover types and water equivalent and other snow properties in Ontario that are useful for snowmelt modeling.

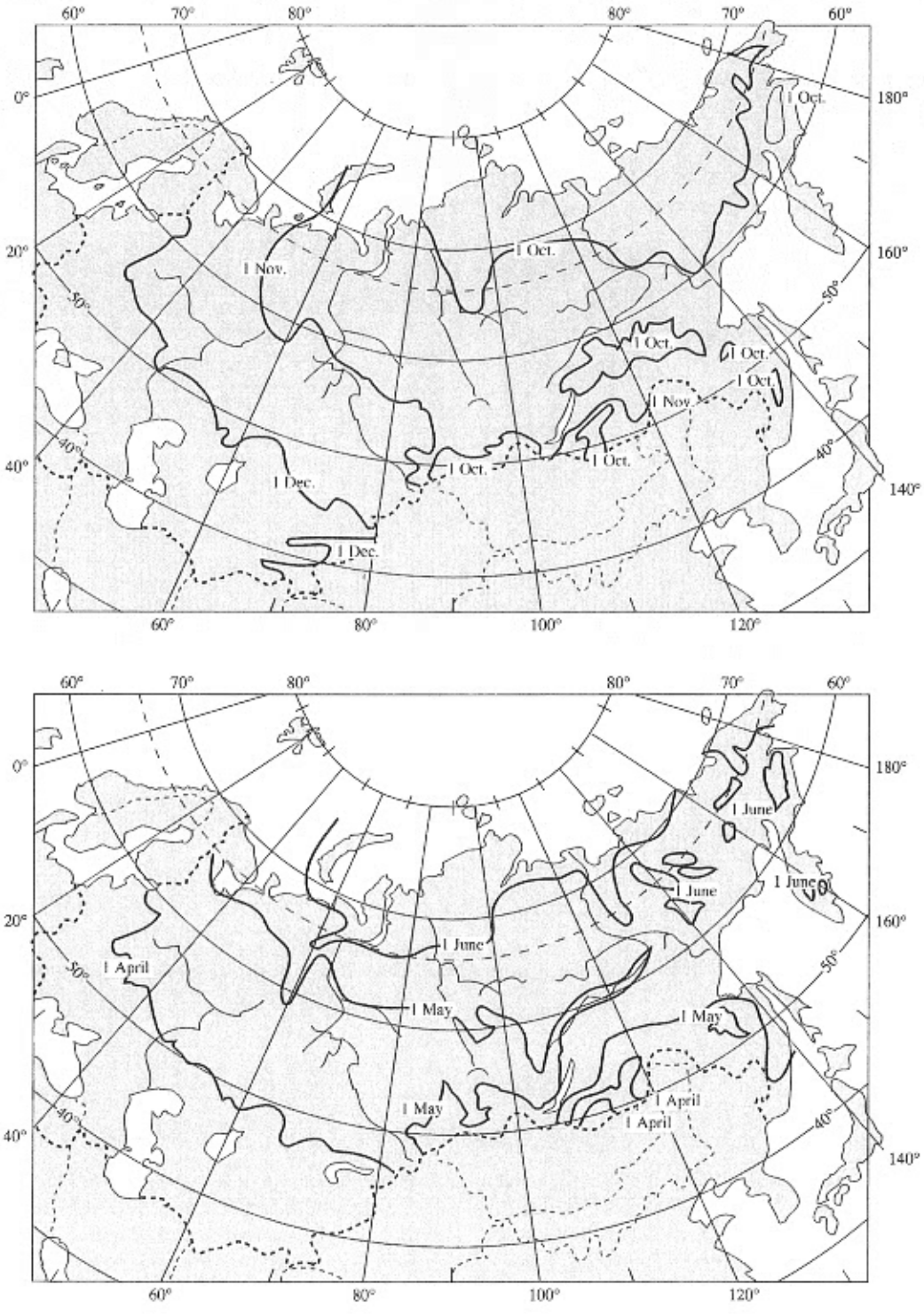

FIGURE 5-13
Average date of snow cover (a) formation and (b) disappearance in the former Soviet Union. From Wilson (1969).

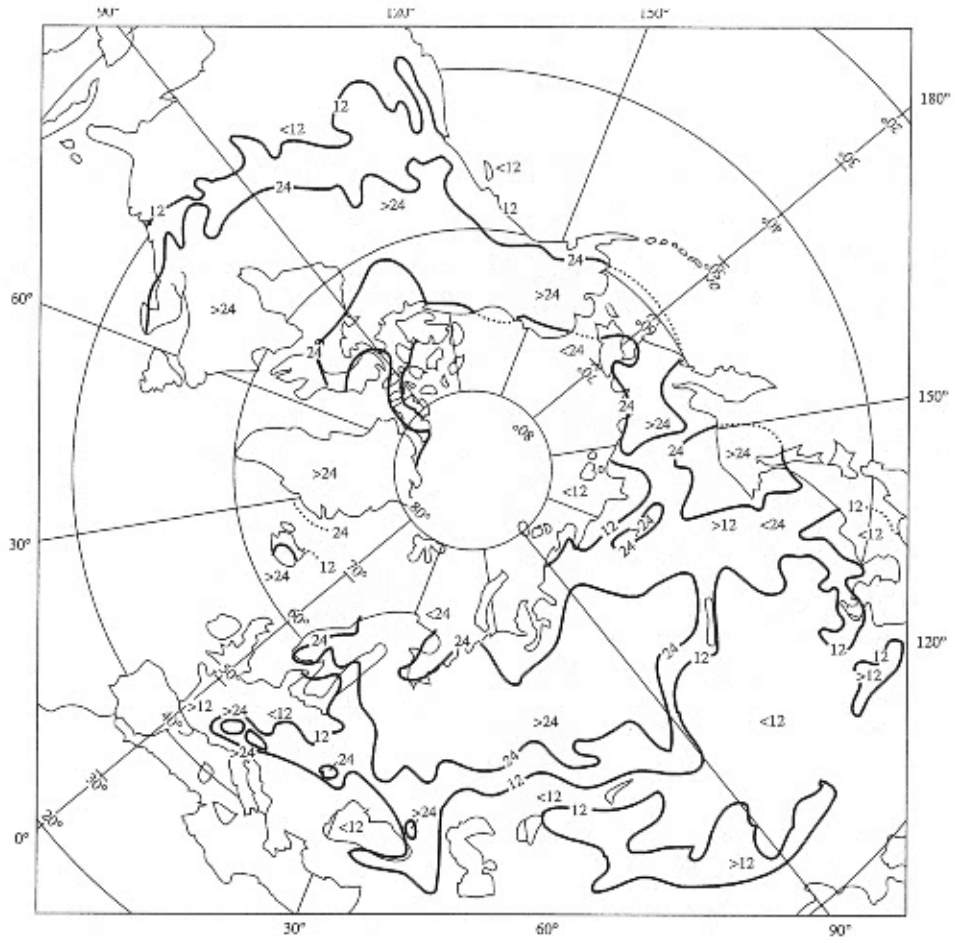

FIGURE 5-14
Average seasonal maximum snow depth (in.) for the northern hemisphere. From Bates and Bilello (1966).

5.4 SNOWMELT PROCESSES[2]

5.4.1 Phases of Snowmelt

The period of general increase of snowpack water equivalent prior to the melt period is called the **accumulation period.** During this period, the net inputs of energy are generally negative and the average snowpack temperature is decreasing; water equivalent typically has an increasing trend during this period. The **melt period** of a seasonal snowpack begins when the net input of energy to it becomes more or less continually positive, and it can usually be separated into three phases:[3]

the **warming phase,** during which the average snowpack temperature increases more or less steadily until the snowpack is isothermal at 0 °C;

[2] Much of our current understanding of snowmelt processes and the forecasting of snowmelt runoff is based on an intensive research program conducted by the U.S. Army Corps of Engineers in the western United States in the early 1950s. The results of this research are extensively summarized in *Snow Hydrology* (U.S. Army Corps of Engineers 1956).

[3] In some regions and during some years, snow covers may form and melt more than once during the winter; in these cases, each successive snowpack will go through an accumulation period and the three phases of the melt period.

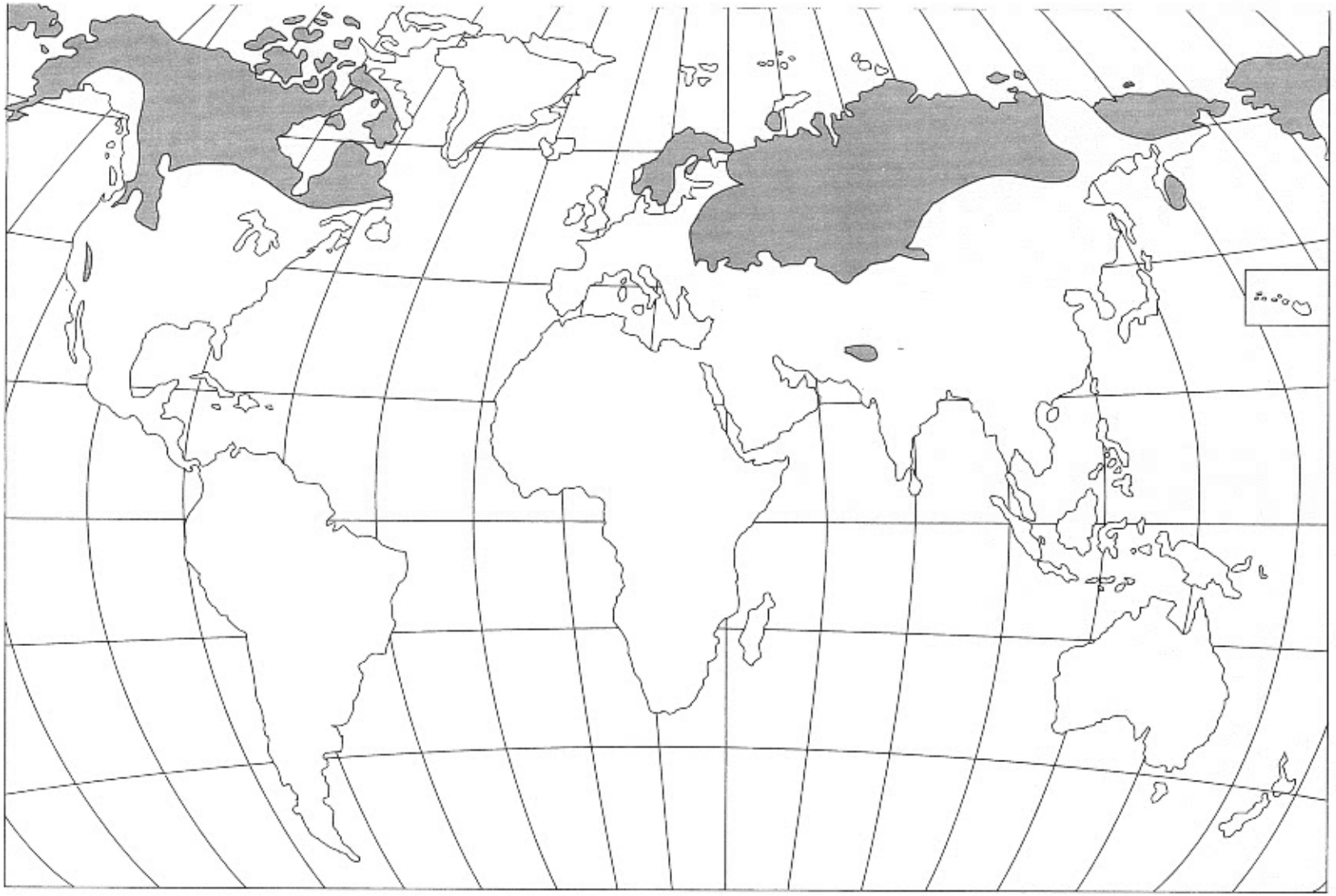

FIGURE 5-15
Regions in which more than half of the annual runoff is derived from snowmelt. From L'vovich (1974); used with permission of the American Geophysical Union.

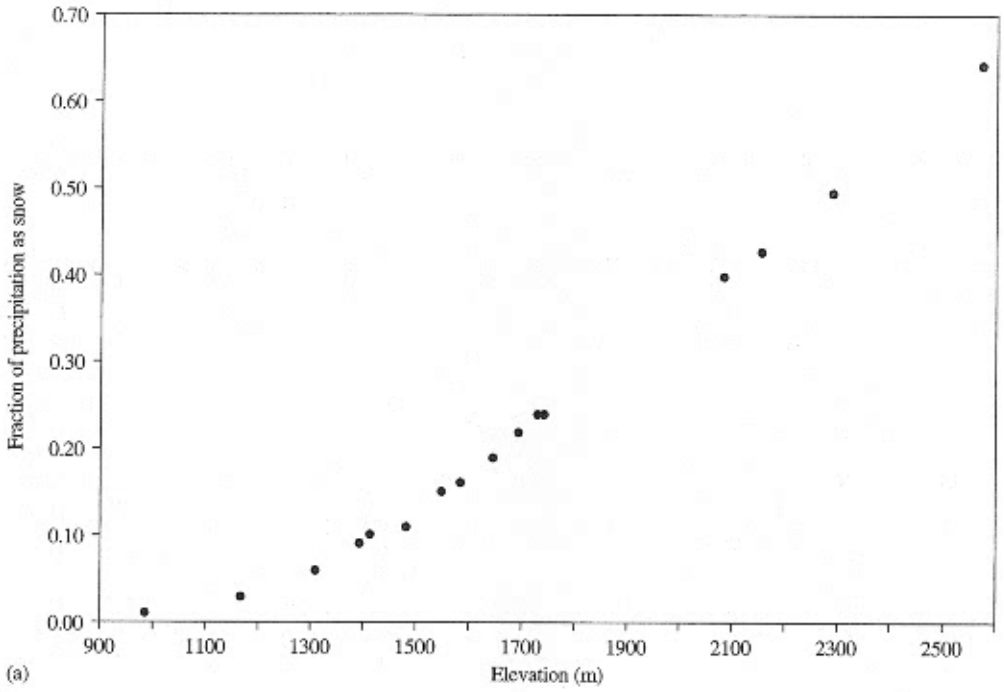

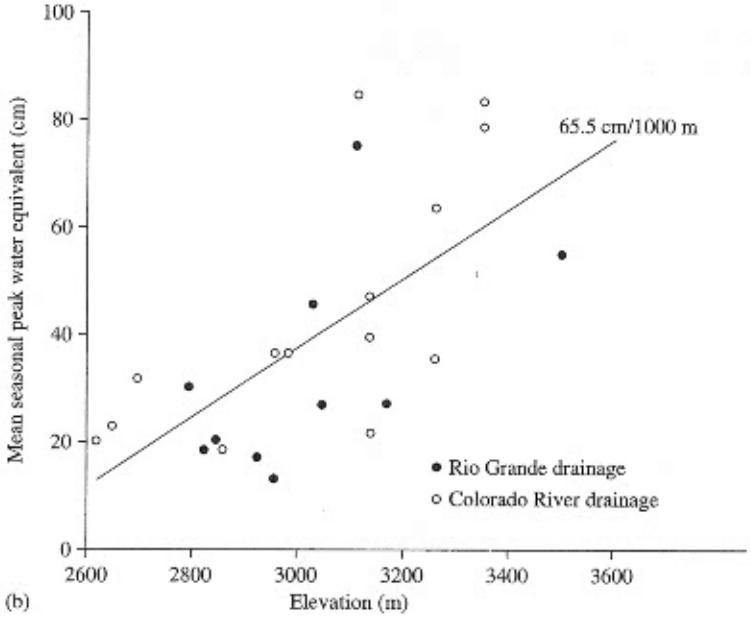

FIGURE 5-16
(a) Fraction of precipitation occurring as snow as a function of elevation in the San Bernardino Mountains of southern California. Data from Minnich (1986). (b) Annual peak water equivalent as a function of elevation, San Juan Mountains, CO, USA. From Caine (1975); used with permission of the American Water Resources Association.

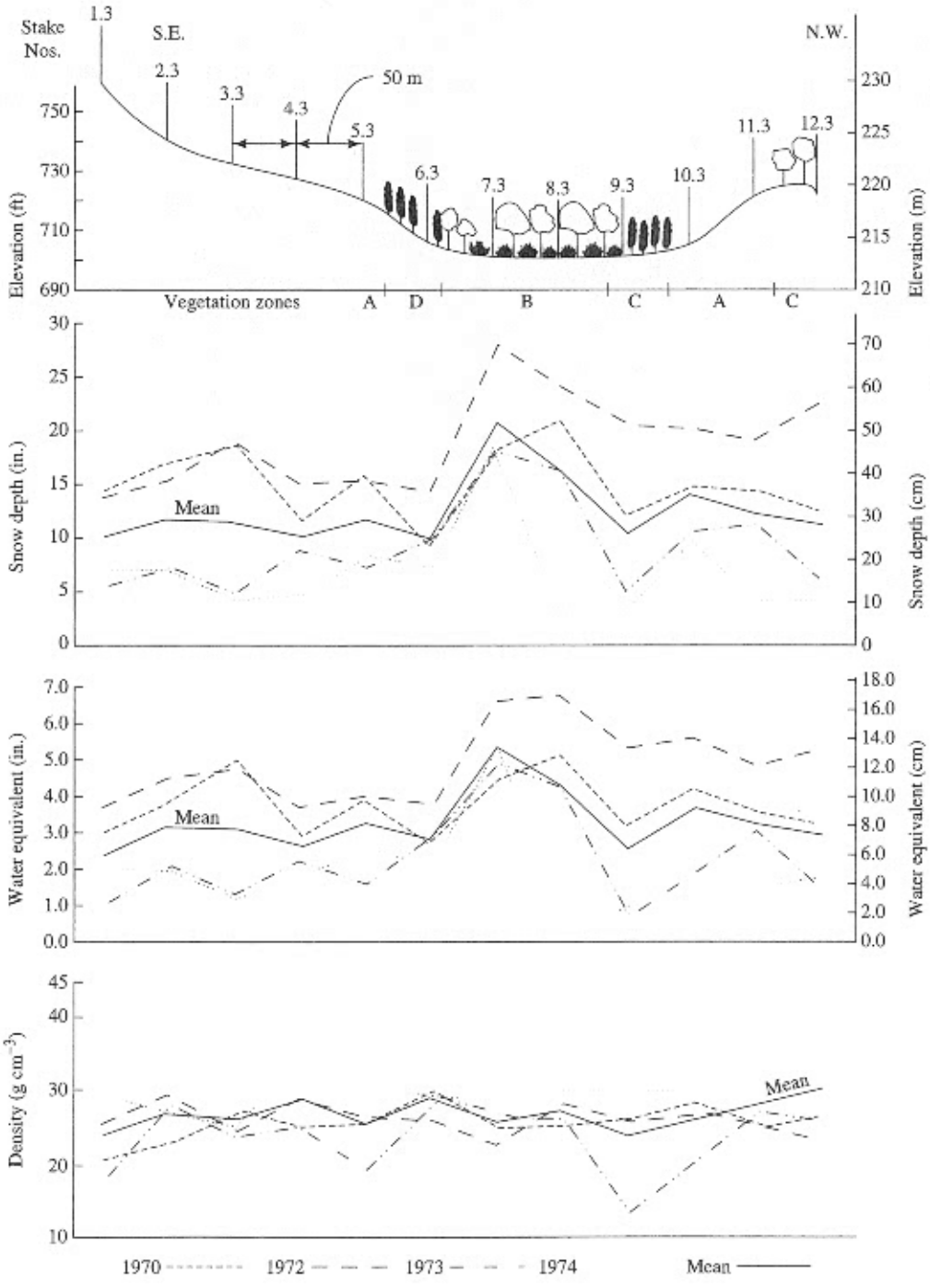

FIGURE 5-17
Peak seasonal snow properties along a transect near Peterborough, Ontario, for four winters. Vegetation Zones: A = grass; B = open deciduous forest with shrubs understory; C = moderately dense deciduous and coniferous forest; D = dense cedar forest. From Adams (1976); used with permission of the American Geophysical Union.

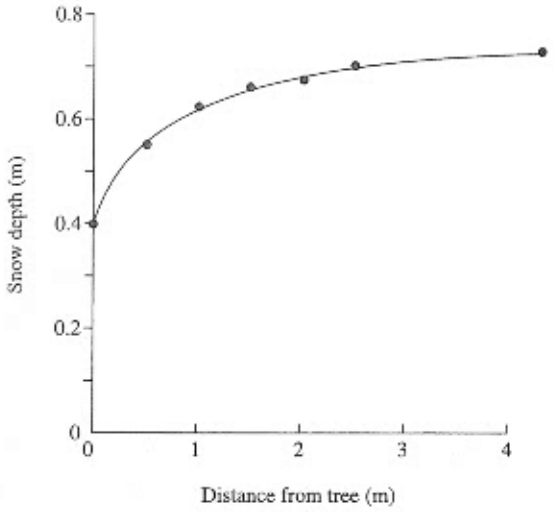

FIGURE 5-18
Snow depth as a function of distance from a tree in a spruce forest in northern Ontario. From data of Woo and Steer (1986).

the **ripening phase,** during which melting occurs, but the meltwater is retained in the snowpack. At the end of this phase, the snowpack is isothermal at 0 °C, cannot retain any more liquid water, and is said to be **ripe**; and

the **output phase,** during which further inputs of energy produce water output.

In many situations, the snowpack does not progress steadily through this sequence. Some melting usually occurs at the surface of a snowpack from time to time prior to the ripening phase, when the air temperature rises above 0 °C for periods of hours or days. The meltwater thus produced percolates into the cold snow at depth and refreezes, releasing latent heat that raises the snow temperature. Similarly, snow-surface temperatures may fall below freezing during the melt period, and the surface layer must warm again before melting can continue. Even where daytime temperatures are continuously above freezing, temperatures commonly fall below 0 °C at night, and it may take several hours for the snowpack to warm and resume melting each day (Bengtsson 1982; Tseng et al. 1994). Nevertheless, the sequence of three phases provides a useful context for understanding the melt process. As described next, the amounts of net energy inputs required for each of the melt phases can be readily computed.

Warming Phase

The **cold content,** Q_{cc}, of a snowpack is the amount of energy required to raise its average temperature to the melting point, so

$$Q_{cc} = -c_i \cdot \rho_w \cdot h_m \cdot (T_s - T_m), \qquad \textbf{(5-13)}$$

where c_i is the heat capacity of ice (2102 J kg^{-1} K^{-1}),[4] T_s is the average temperature of the snowpack, T_m is the melting-point temperature (0 °C), and the other symbols are as previously defined. The cold content can be computed at any time prior to the ripening phase, and the net energy input required to complete phase 1, Q_{m1}, equals the cold content at the beginning of the melt period. Note that Q_{cc} has dimensions [E L^{-2}].

EXAMPLE 5-2

Given a snowpack with the average conditions computed in Example 5-1 and an average temperature of –9 °C, what is its cold content?

Solution The constants in Equation (5-13) have the following values: $c_i = 2102$ J kg^{-1} K^{-1}, $\rho_w = 1000$ kg m^{-3}, and $T_m = 0$ °C. From Example 5-1, $h_m = 29$ cm $= 0.29$ m and $T_s = -9$ °C. Substituting these values in Equation (5-13) yields

$$\begin{aligned} Q_{cc} = &-2102 \text{ J kg}^{-1} \text{ K}^{-1} \\ &\times 1000 \text{ kg m}^{-3} \times 0.29 \text{ m} \\ &\times (-9°\text{C} - 0°\text{C}) = 5.49 \text{ MJ m}^{-2} \end{aligned}$$

as the net input of energy required to raise this snowpack to the melting point.

Ripening Phase

Phase 2 of melting begins when the snowpack becomes isothermal at 0 °C. After this time, further net inputs of energy produce meltwater, which is initially retained in the pore spaces by surface-tension forces (Figure 5-19). The liquid-water-retaining capacity, h_{wret}, of a snowpack is given by

$$h_{wret} = \theta_{ret} \cdot h_s, \qquad \textbf{(5-14)}$$

[4] Since the Kelvin and Celsius temperature scales have identical degree intervals and differ only in the location of the zero point, units involving temperature intervals have identical values in both scales; that is, 2102 J kg^{-1} K^{-1} = 2102 J kg^{-1} °C^{-1}. (See Example A-7.)

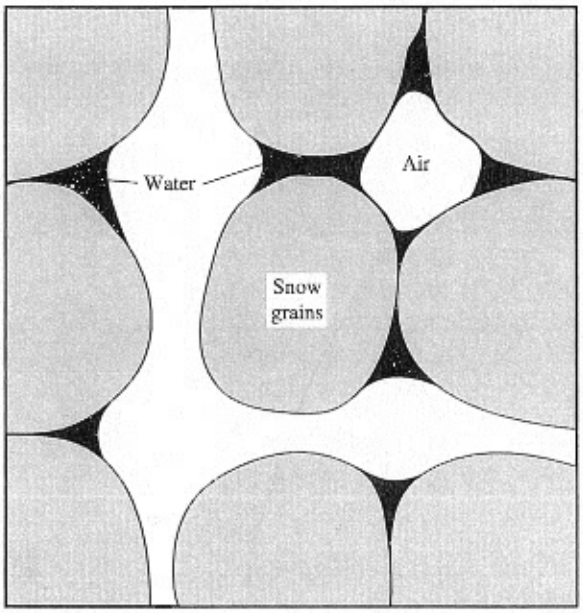

FIGURE 5-19
An idealized thin section of snow showing snow grains, water retained by surface tension, and continuous pores filled with air. After Colbeck (1971).

where θ_{ret} is the maximum volumetric water content that the snow can retain against gravity.[5] θ_{ret} for ripe snow can be estimated from empirical studies summarized by Eagleson (1970) as

$$\theta_{ret} = -0.0735 \cdot \left(\frac{\rho_s}{\rho_w}\right) + (2.67 \times 10^{-4}) \cdot \left(\frac{\rho_s^2}{\rho_w}\right), \quad \textbf{(5-15)}$$

where the densities are in kg m^{-3}. This relation is graphed in Figure 5-20.

We can use previously derived expressions to compute the proportion of pore spaces that are filled with water when $\theta = \theta_{ret}$. Consider a typical ripe snowpack with $\rho_s = 500$ kg m^{-3}. Equation (5-15) gives $\theta_{ret} = 0.03$. Substituting these quantities into Equation (5-6) allows us to compute the corresponding porosity $\phi = 0.49$. The ratio θ_{ret}/ϕ is the proportion of pore spaces filled with water at the end of phase 2 [see Equations (5-2) and (5-4)], which for this case is 0.03/0.49 = 0.061. Thus it is clear that only about 6% of the pore spaces in a ripe snowpack contain water, and such snowpacks are far from being saturated.

The net energy input required to complete the ripening phase, Q_{m2}, can be computed as

$$Q_{m2} = h_{wret} \cdot \rho_w \cdot \lambda_f = \theta_{ret} \cdot h_s \cdot \rho_w \cdot \lambda_f, \quad \textbf{(5-16)}$$

where λ_f is the latent heat of fusion (0.334 MJ kg^{-1}).

EXAMPLE 5-3

Assume that the snowpack considered in Examples 5-1 and 5-2 has become isothermal at the melting point and its density has increased to 400 kg m^{-3}. How much energy is required to bring it to a ripe condition?

Solution Assuming the water equivalent has not changed, the current snow depth is 72.5 cm [Equation (5-12)]. From Equation (5-15), $\theta_{ret} = 0.013$. With $\lambda_f = 0.334$ MJ kg^{-1}, we compute

$$Q_{m2} = 0.013 \times 0.725 \text{ m} \times 1000 \text{ kg m}^{-3} \times 0.334 \text{ MJ kg}^{-1} = 3.15 \text{ MJ m}^{-2}$$

via Equation (5-16).

Output Phase

Once the snowpack is ripe, further net energy inputs produce meltwater that cannot be held by surface-tension forces against the pull of gravity, and water begins to percolate downward, ultimately to become water output. This flow is more fully described in Section 5.4.3.

The net energy input required to complete the output phase, Q_{m3}, is the amount of energy needed to melt the snow remaining at the end of the ripening phase:

$$Q_{m3} = (h_m - h_{wret}) \cdot \rho_w \cdot \lambda_f. \quad \textbf{(5-17)}$$

5.4.2 The Energy Balance

Consider again the representative element of a snowpack shown in Figure 5-1. The energy balance for this element is

$$\Delta t \cdot S = \Delta Q, \quad \textbf{(5-18)}$$

where S [E L^{-2} T^{-1}] is the net rate of energy exchanges into this element by all processes over a

[5] θ_{ret} is directly analogous to the "field capacity" of a soil, defined in Section 6.4.1.

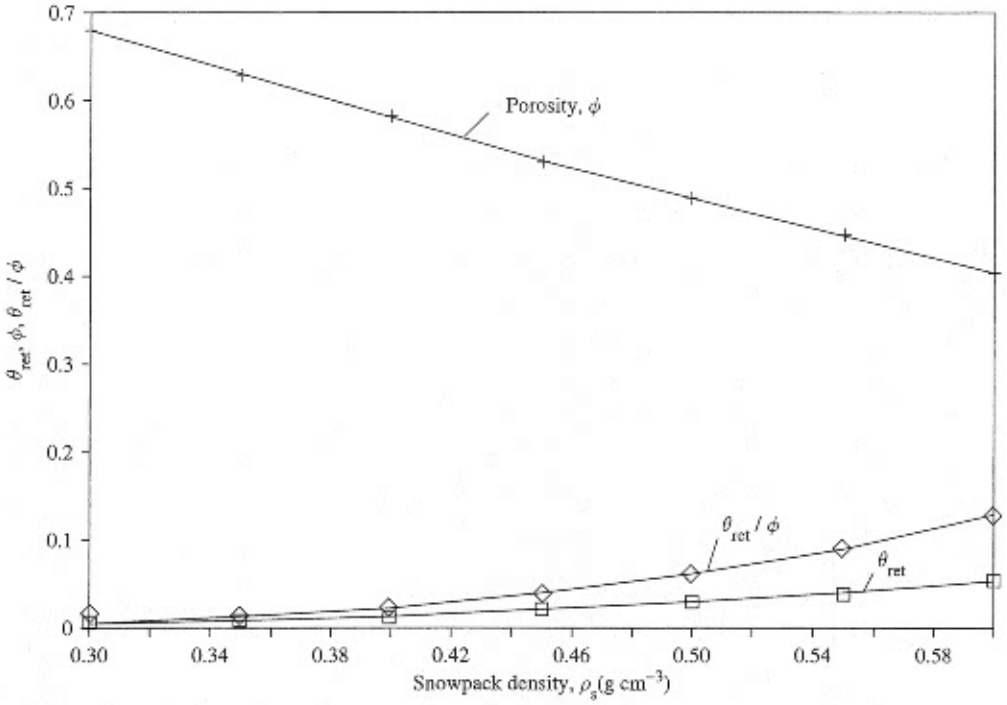

FIGURE 5-20
Empirical relations between porosity, ϕ, and relative snow density, ρ_s/ρ_w [Equation (5-6)]; liquid-water-holding capacity, θ_{ret}, and ρ_s [Equation (5-15)]; and θ_{ret}/ϕ and ρ_s/ρ_w. From data plotted in Eagleson (1970).

time period Δt [T], and ΔQ [E L^{-2}] is the change in heat energy absorbed by the snowpack during Δt.

The equations developed in this section provide a means of modeling the progress of snowmelt based on information about the net rate of energy input, S, during successive time periods. This approach to modeling is explicitly explored in Section 5.5.1. The several components of S and the ways in which their magnitudes can be estimated are discussed later in this section.

During the warming phase, ΔQ is reflected in an increase in average temperature of the snowpack, ΔT_s:

$$\Delta Q = c_i \cdot \rho_w \cdot h_m \cdot \Delta T_s. \qquad \textbf{(5-19)}$$

[Compare Equation (5-19) with Equation (5-13).] Substitution of Equation (5-19) into Equation (5-18) relates the temperature change to the net rate of energy inputs:

$$\Delta T_s = \frac{\Delta t \cdot S}{c_i \cdot \rho_w \cdot h_m}. \qquad \textbf{(5-20)}$$

In the second and third phases, ΔQ is reflected in melting. During the ripening phase, this melting causes an increase in the liquid water held in the snowpack, so

$$\Delta Q = \rho_w \cdot \lambda_f \cdot \Delta h_w \qquad \textbf{(5-21)}$$

and

$$\Delta h_w = \frac{\Delta t \cdot S}{\rho_w \cdot \lambda_f}. \qquad \textbf{(5-22)}$$

During the output phase,

$$\Delta Q = -\rho_w \cdot \lambda_f \cdot \Delta h_m, \qquad \textbf{(5-23)}$$

so

$$\Delta h_m = -\frac{\Delta t \cdot S}{\rho_w \cdot \lambda_f} \qquad \textbf{(5-24)}$$

and

$$\Delta w = -\Delta h_m, \qquad \textbf{(5-25)}$$

where Δw is the increment of water output from the snowpack.

EXAMPLE 5-4

Given a ripe snowpack, compute the amount of water output produced on a day when the total net energy input, S, is 5.11 MJ m^{-2}.

Solution According to Equations (5-24) and (5-25),

$$\Delta w = \frac{1 \text{ day} \times 5.11 \text{ MJ m}^{-2} \text{ day}^{-1}}{1000 \text{ kg m}^{-3} \times 0.334 \text{ MJ kg}^{-1}}$$
$$= 0.0153 \text{ m} = 15.3 \text{ mm}.$$

Energy-Exchange Processes

The energy exchanges that determine the progress of snowmelt occur via the following processes (the symbols will be used to represent the net rates of energy input, or **fluxes,** [$E L^{-2} T^{-1}$], by each process):

shortwave (solar) radiation input, K;

longwave radiation exchange, L;

turbulent exchange of sensible heat with the atmosphere, H;

turbulent exchange of latent heat with the atmosphere, LE;

heat input by rain, R;

conductive exchange of sensible heat with the ground, G.

Thus,

$$S = K + L + H + LE + R + G. \quad \textbf{(5-26)}$$

The basic physics of each of these components of the energy budget, and the approaches to determining their magnitudes, are discussed in the following sections.

Shortwave Radiation Input As indicated in Figure 3-1, the sun's energy is electromagnetic radiation with wavelengths less than 4 μm; most of this energy is concentrated between 0.4 and 0.7 μm wavelength. K is the net flux of solar energy entering the snowpack, so

$$K = K_{in} - K_{out} = K_{in} \cdot (1 - a), \quad \textbf{(5-27)}$$

where K_{in} is the flux of solar energy incident on the snowpack surface, K_{out} is the reflected flux, and a is the shortwave reflectance, or albedo (see Table D-2).[6]

K includes both the energy in the direct solar beam and the diffuse solar radiation due to scattering by atmospheric gases and aerosols (Section E.1). The diffuse component makes up about 10% of total incident shortwave radiation under clear-sky conditions, increasing to 100% when there is complete overcast (Hay 1976). However, the diffuse component is difficult to estimate, and since it seldom accounts for more than a small fraction of the total energy balance, we will not treat it separately in our development.

K can be measured with instruments called **pyranometers** [described in Iqbal (1983)], one facing upward to measure K_{in} and one downward to measure K_{out} in a representative location. However, pyranometers and the associated data loggers are installed at only a few permanent locations (see Figures E-1 and E-2) and research stations, so that it is common to estimate K. To do this, we note that K_{in} represents the clear-sky shortwave radiation flux, K_{cs}, adjusted for the slope and aspect (i.e., the azimuth of a line running downslope) of the land surface and reduced by cloud cover and shading by vegetation:

$$K_{in} = K_{cs}(\Lambda, J) \cdot f_1(\Lambda, \beta, \alpha) \cdot f_2(C) \cdot f_3(F). \quad \textbf{(5-28)}$$

Here, Λ is the latitude, J is the day of year (the number of days since the calendar year began), β is the slope inclination angle, α is the slope azimuth angle (measured clockwise from north), C is the fraction of sky covered with clouds, F is the fraction of sky obscured by forest canopy, and f_1, f_2, and f_3 are functions expressing the effects of the quantities in parentheses.

Combining Equations (5-27) and (5-28), we have

[6] The albedo equals the integrated reflectance for shortwave radiation, for which the symbol $\rho(\lambda)$ is used in Section D.1 [Equation (D-4)]. The symbol a is used for albedo throughout the text to avoid confusion with the symbol used for densities.

$$K = K_{cs}(\Lambda, J) \cdot f_1(\Lambda, \beta, \alpha) \cdot f_2(C) \cdot f_3(F) \cdot (1 - a). \quad \textbf{(5-29)}$$

Methods for estimating the quantities in Equation (5-29) are outlined next.

Clear-Sky Shortwave Radiation The complete set of equations and the algorithm for computing clear-sky shortwave radiation on horizontal and sloping surfaces without vegetative cover are given in Appendix E; only the general approach is described here.

The total daily flux of clear-sky radiation falling on a horizontal surface is a function of the latitude (Λ) and the declination angle (δ) of the sun, which is a function of the time of year (J). At a given latitude, this quantity varies approximately sinusoidally through the year (Figure 5-21).

As anyone living in a region with seasonal snow cover knows, there is a great difference between the amounts of solar radiation received on north- and south-facing slopes. This difference is illustrated by the data in Table 5-2, which compares the clear-sky shortwave radiation inputs on north- and south-facing slopes at Danville, VT, during the snowmelt season. The function $f_1(\Lambda, \beta, \alpha)$ is derived using the concept of **equivalent latitude** and is given in Section E.2.

Effect of Cloud Cover The effect of cloud cover can be estimated using empirical relations such as

$$f_2(C) = 0.355 + 0.68 \cdot (1 - C). \quad \textbf{(5-30)}$$

This expression was used successfully by Croley (1989) in predicting evaporation from lakes; the U.S. Army Corps of Engineers (1956) suggested an alternative relation involving cloud height:

$$f_2(C) = 1 - (1 - k_s) \cdot C. \quad \textbf{(5-31)}$$

In this equation,

$$k_s = 0.18 + (7.9 \times 10^{-5}) \cdot Z_C, \quad \textbf{(5-32)}$$

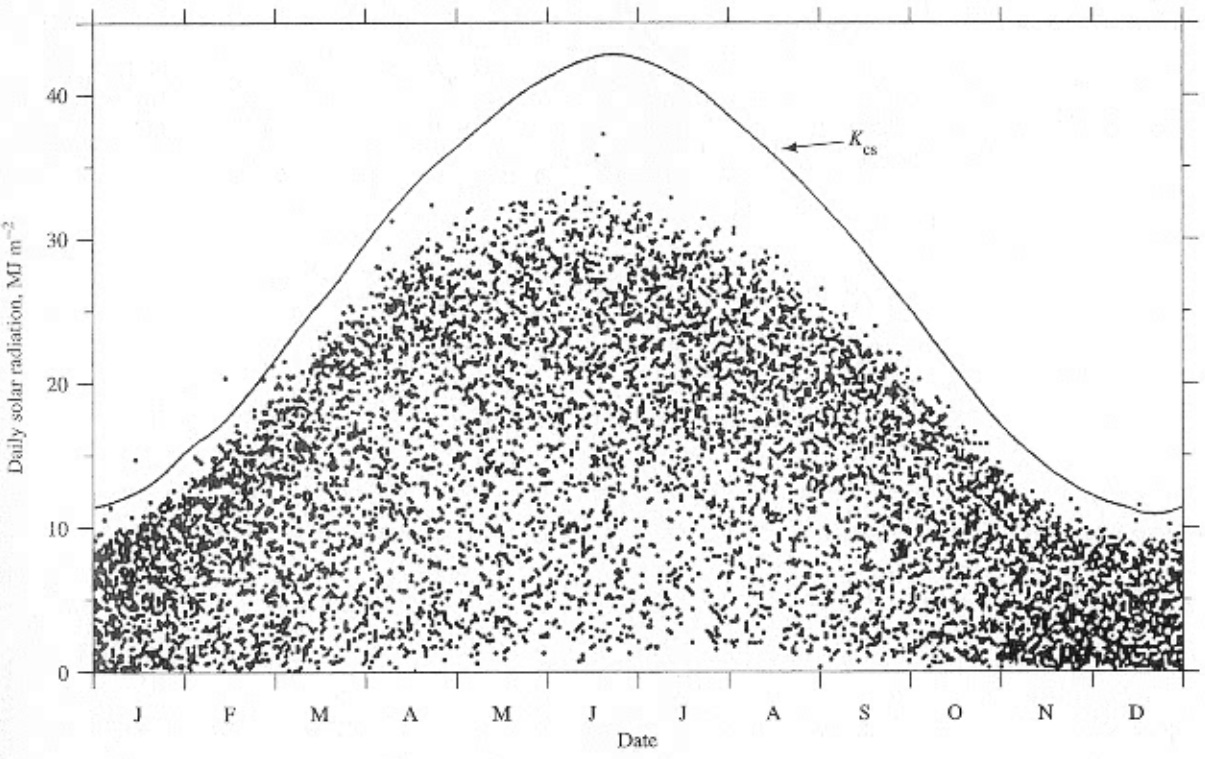

FIGURE 5-21
Clear-sky (potential), K_{cs}, and incident, K_{sy}, solar radiation on a horizontal surface at West Thornton, NH, for 1960 through 1987. Each dot represents measured K_{sy} for a day. From Federer et al. (1990).

TABLE 5-2
Total Daily Incident Clear-Sky Solar Radiation Received on North- and South-Facing Slopes of Varying Inclinations at Danville, VT (latitude 44.5° N) on 17 March (MJ m^{-2}).

Slope Inclination Angle, β (°)	North-facing slope (α = 0°)	South-facing slope (α = 180°)
0	20.6	20.6
5	18.7	22.4
10	16.6	24.1
15	14.3	25.5
20	12.0	26.8
25	9.5	27.9
30	7.0	28.7
35	4.5	29.3
40	1.9	29.7

where Z_C is height of the cloud base in meters.

A slightly different approach to estimating the effect of cloud cover is based on the ratio of the "percentage of possible sunshine," which is the ratio of the duration of bright sunshine during a day to the length of time between sunrise and sunset. A nomograph for this approach was developed by Hamon et al. (1954).

However, manual observations of C are no longer available in the United States because human weather observers are being replaced by automated stations. Because of this fact, Lindsey and Farnsworth (1997) recommended that, where K_{in} is not directly measured, it is best determined from gridded estimates of solar radiation developed from Geostationary Operational Environmental Satellite (GOES) imagery. Useful estimates of K_{in} can also be developed using daily maximum and minimum temperature and precipitation data (Hunt et al. 1998).

Effect of Forest Canopy The value of F can be determined as the ratio of the horizontally projected area of forest canopy to the total area of interest and is best determined from air photographs. Figure 5-22 shows values of $f_3(F)$ for four types of conifer forest. No comparable data for other forest types seem to have been published, and because the effect of vegetative cover in reducing incident shortwave radiation depends on the type, height, and spacing of the plants, these relations must be applied with caution for other situations. The relationship for lodgepole pine can be approximated as

$$f_3(F) = \exp(-3.91 \cdot F). \qquad \textbf{(5-33)}$$

Albedo As shown in Table D-2, snowpack albedo ranges from about 0.45 for old snow to about 0.85 for a fresh snow surface; thus this factor is an important determinant of the net input of energy to the snowpack. Figure 5-23 shows the empirical relation between albedo and the age of snow surface for the melt and accumulation seasons as measured by the U.S. Army Corps of Engineers (1956); these curves are commonly used in energy-balance models of snow melt.

Because of the porous nature of snow, solar radiation is reflected not at the surface plane, but over a finite depth. Studies have shown that there is little penetration of solar radiation below about 10 cm,

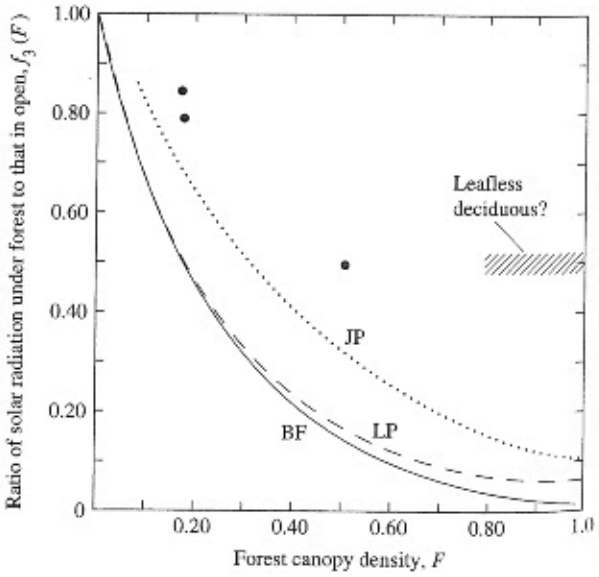

FIGURE 5-22
Ratio of incident solar radiation under various types of forest canopies to that received in the open for four forest types: BF = balsam fir, JP = jack pine, LP = lodgepole pine, circles = open boreal spruce forest. From *Water in Environmental Planning*, by Thomas Dunne and Luna B. Leopold. Copyright © 1978 by W.H. Freeman and Company. Reprinted with permission.

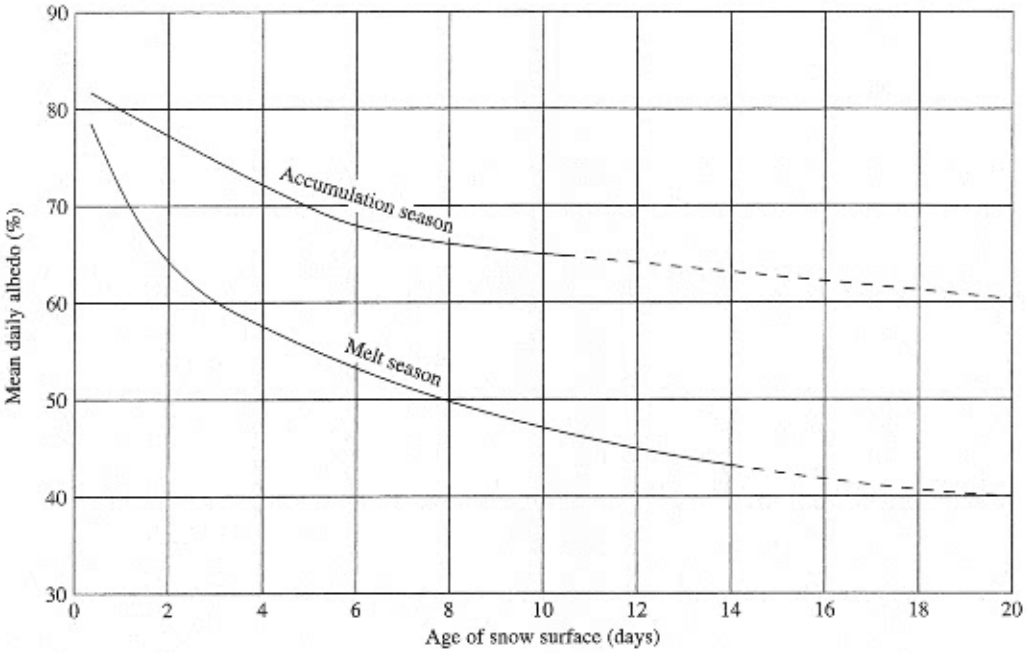

FIGURE 5-23
Albedo as a function of age of snow surface (i.e., time since last snowfall). From U.S. Army Corps of Engineers (1956).

so Figure 5-23 applies only when $h_s > 10$ cm. For shallower snowpacks, significant amounts of radiation are absorbed by the ground and may heat the snow from below. Leonard and Eschner (1968) found that albedo measured for snow intercepted on a conifer forest was considerably lower ($a \approx 0.2$) than for a ground snowpack, resulting in more rapid melting and greater evaporation for intercepted snow.

Summary The following example shows how net solar radiation flux to a snowpack is typically estimated by use of the preceding relationships.

EXAMPLE 5-5

Compute the total daily net input of solar radiation, K, to a snowpack in a conifer forest with a canopy closure of $F = 0.8$ on a north-facing slope with an inclination of 20° on 17 March at the latitude of Danville, VT. The cloud cover is 0.5, and the last snow storm occurred on 12 March.

Solution The product of the first two terms in Equation (5-29) can be found in Table 5-2 as 14.3 MJ m^{-2} day^{-1}. (For other days, locations, slopes, and aspects, we would use the relations given in Appendix E.) We compute $f_2(C)$ using Equation (5-30) and $f_3(F)$ using Equation (5-33):

$$f_2(C) = 0.355 + 0.68 \times (1 - 0.5) = 0.695;$$
$$f_3(F) = \exp(-3.91 \times 0.8) = 0.044.$$

Since the snowpack age is 5 days, the albedo estimated from Figure 5-23 is $a = 0.55$. Substituting all these values into Equation (5-29) gives

$$K = 14.3 \text{ MJ m}^{-2} \times 0.695 \times 0.044 \times (1 - 0.55) = 0.20 \text{ MJ m}^{-2} \text{ day}^{-1}.$$

Longwave Radiation Exchange Longwave, or terrestrial, radiation is electromagnetic radiation with wavelengths of 4 to 20 μm emitted by materials at near-earth-surface temperatures. (See Figure 3-1 and Section D.1.) The net input of longwave energy, L, is the difference between the incident flux, L_{in}, emitted by the atmosphere, clouds, and overlying forest canopy and the outgoing radiation from the snowpack, L_{out}:

$$L = L_{in} - L_{out}. \quad \textbf{(5-34)}$$

Longwave radiation can be measured directly by means of **pyrgeometers**; alternatively, it can be

found as the difference between all-wave radiation measured by a **radiometer** and shortwave radiation measured by a pyranometer. However, such instruments are seldom installed except at sites of intensive research, and routine measurements of longwave radiation are available at only a few locations. Thus, as with shortwave radiation, one is usually forced to estimate the longwave component of the energy balance from more readily available meteorological information; this estimation is based on the considerations described next.

The flux of electromagnetic radiation emitted by a surface is given by the Stefan-Boltzmann equation [Equation (D-1)]. Hence we can write

$$L_{in} = \varepsilon_{at} \cdot \sigma \cdot (T_{at} + 273.2)^4, \qquad \textbf{(5-35)}$$

where ε_{at} is the integrated effective emissivity of the atmosphere and canopy, σ is the Stefan-Boltzmann constant ($\sigma = 4.90 \times 10^{-9}$ MJ m^{-2} day^{-1} K^{-4}), and T_{at} is the effective radiating temperature of the atmosphere and canopy (°C). The outgoing flux is the sum of the radiation emitted by the snow surface and the portion of the incident radiation reflected by the surface. Since the longwave reflectivity of a surface equals one minus its longwave emissivity, we have

$$L_{out} = \varepsilon_{ss} \cdot \sigma \cdot (T_{ss} + 273.2)^4 + (1 - \varepsilon_{ss}) \cdot L_{in}, \qquad \textbf{(5-36)}$$

where the subscript *ss* designates the values of emissivity and temperature for the snow surface.

Combining Equations (5-34), (5-35), and (5-36) and expanding and simplifying gives

$$L = \varepsilon_{ss} \cdot \varepsilon_{at} \cdot \sigma \cdot (T_{at} + 273.2)^4 - \varepsilon_{ss} \cdot \sigma \cdot (T_{ss} + 273.2)^4; \qquad \textbf{(5-37a)}$$

however, since the emissivity of snow is very close to 1 (Table D-1), Equation (5-37a) can be simplified to

$$L = \varepsilon_{at} \cdot \sigma \cdot (T_{at} + 273.2)^4 - \sigma \cdot (T_{ss} + 273.2)^4. \qquad \textbf{(5-37b)}$$

The major problem in applying Equation (5-37) is to find expressions for ε_{at} and T_{at} or, equivalently, to estimate the value of L_{in} under various conditions of cloudiness and forest cover. This problem is addressed in the following sections.

Clear-Sky Longwave Radiation Expressions for estimating L_{in} are usually developed by noting that the most important absorbers and emitters of longwave radiation in the atmosphere are carbon dioxide and water vapor (Figure 3-1). Since the concentration of carbon dioxide is quite constant over time periods of interest to snowmelt modeling, variations in the downward flux of longwave radiation under clear skies and no forest canopy are due largely to fluctuations in humidity. Several empirical functions expressing this relation have been developed; we select one that was derived from considering the vertical distribution of water vapor in the atmosphere (Brutsaert 1975):

clear sky, no forest canopy

$$\varepsilon_{at} = 1.72 \cdot \left(\frac{e_a}{T_a + 273.2} \right)^{1/7}, \qquad \textbf{(5-38)}$$

where e_a is near-surface (2-m height) atmospheric vapor pressure (kPa) and T_a is 2-m air temperature (°C).

Effect of Cloud Cover Clouds are black bodies emitting longwave radiation at a rate determined by the temperature of the cloud base, and their presence greatly increases the effective emissivity of the atmosphere. Thus under cloudy conditions ε_{at} will be determined by the degree of cloud cover, C; an approximate empirical equation expressing this relation was given by Kustas et al. (1994):

cloudy sky, no forest canopy

$$\varepsilon_{at} = 1.72 \cdot \left(\frac{e_a}{T_a + 273.2} \right)^{1/7} \cdot (1 + 0.22 \cdot C^2). \qquad \textbf{(5-39)}$$

Effect of Forest Canopy As is the case with clouds, trees are very nearly blackbodies with respect to longwave radiation (Table D-1), and they can be considered to be emitting radiant energy at a rate determined by their temperature. Since their temperature is close to the near-surface air temperature, their effect on the total integrated atmospheric emissivity can be modeled as in Equation (5-40):

cloudy sky, forest canopy (general equation)

$$\varepsilon_{at} = (1 - F) \cdot 1.72 \cdot \left(\frac{e_a}{T_a + 273.2} \right)^{1/7} \cdot (1 + 0.22 \cdot C^2) + F. \qquad \textbf{(5-40)}$$

Here, F is as defined for shortwave radiation. Note that Equation (5-40) is general; it reduces to Equation (5-39) for cloudy conditions with no forest canopy and to Equation (5-38) for clear-sky conditions with no canopy.

Longwave Radiation Emitted by Snow Surface The second term on the right side of Equation (5-37) is the radiation flux emitted by the snow surface. Brubaker et al. (1996) showed that the average daily snow-surface temperature is well approximated by

$$T_{ss} = \min[(T_a - 2.5), 0], \qquad \textbf{(5-41)}$$

where temperatures are in °C. During phases 2 and 3 of melting, the snow surface is at the freezing point: $T_{ss} = 0$ °C.

Summary The foregoing discussion indicates that, in practice, $T_{at} = T_a$, and, when $T_a > 0$ °C, $T_{ss} = 0$ °C and Equation (5-37b) becomes

$$L \approx \varepsilon_{at} \cdot \sigma \cdot (T_a + 273.2)^4 - 27.3, \qquad \textbf{(5-42)}$$

where the energy fluxes are in MJ m^{-2} day^{-1}.

In most situations, $\varepsilon_{at} < 1$ and L is negative. However, ε_{at} can be > 1 and L can be positive if the air temperature and cloud cover or forest cover have large values. Example 5-6 depicts a case in which the latter situation occurs.

EXAMPLE 5-6

Compute the net longwave radiation exchange, L, for the situation described in Example 5-5, assuming a ripe snowpack, an air temperature, T_a, of 4 °C, and a relative humidity, W_a, of 0.80.

Solution We use Equation (5-40) to compute the atmospheric emissivity ε_{at}. To do this, we must first compute the vapor pressure e_a. From Equation (D-7), we find that the saturation vapor pressure, e_a^*, is

$$e_a^* = 0.611 \text{ kPa} \times \exp\left(\frac{17.3 \times 4^\circ\text{C}}{4^\circ\text{C} + 237.3^\circ\text{C}}\right) = 0.814 \text{ kPa},$$

and from Equation (D-10), we find that the actual vapor pressure is

$$e_a = 0.80 \times 0.814 \text{ kPa} = 0.651 \text{ kPa}.$$

Then

$$\varepsilon_{at} = (1 - 0.80) \times 1.72 \times \left(\frac{0.651}{4 + 273.2}\right)^{1/7} \times (1 + 0.22 \times 0.5^2) + 0.80 = 0.953.$$

We now use this value in Equation (5-42):

$$L = 0.953 \times 4.90 \times 10^{-9} \text{ MJ m}^{-2} \text{ day}^{-1} \text{ K}^{-4} \times [(4 + 273.2) \text{ K}]^4 - 27.3 \text{ MJ m}^{-2} \text{ day}^{-1} = 0.27 \text{ MJ m}^{-2} \text{ day}^{-1}.$$

Turbulent Exchange of Sensible Heat with the Atmosphere The physics of sensible-heat exchange near the earth's surface is developed in Section D.6, leading to Equation (D-49) for neutral atmospheric conditions:

$$H = -\rho_a \cdot c_a \cdot \frac{k^2}{\left[\ln\left(\frac{z_a - z_d}{z_0}\right)\right]^2} \cdot v_a \cdot (T_a - T_s). \qquad \textbf{(D-49)}$$

Here, ρ_a is the density of air, c_a is the heat capacity of air, $k = 0.4$, z_d is the zero-plane displacement height, z_0 is the surface-roughness height, v_a is the windspeed, T_a is the air temperature, z_a is the height above the snow surface at which v_a and T_a are measured, and T_s is the surface temperature.

To modify this equation for snow, we first drop the minus sign, since we consider energy inputs as positive. Second, we can assume that z_d is negligibly small. The roughness height, z_0, depends on the irregularity of the snow surface and thus can be highly variable from place to place and with time at a given location. For example, Anderson (1976) measured values between 0.0001 and 0.038 m for his research site in Vermont. However, his data show a strong decrease in z_0 as the season progressed, and values during the melt season did not exceed 0.005 m. In the absence of other information, a value between 0.0005 and 0.005 m may be selected; however, it should be noted that for special situations, such as vegetation projecting above the snow surface or patchy snow, z_0 could be considerably higher.

With the preceding modifications, and assuming $z_a = 2.00$ m, $z_0 = 0.0015$ m, $c_a = 0.00101$ MJ kg^{-1} K^{-1}, and $\rho_a = 1.29$ kg m^{-3}, Equation (D-49) becomes

$$H = (4.03 \times 10^{-6}) \cdot v_a \cdot (T_a - T_{ss}) \text{ MJ m}^{-2} \text{ s}^{-1}, \quad \textbf{(5-43a)}$$

or

$$H = 0.348 \cdot v_a \cdot (T_a - T_{ss}) \text{ MJ m}^{-2} \text{ day}^{-1}, \quad \textbf{(5-43b)}$$

where v_a is in m s^{-1} and temperatures are in °C.

There are two additional considerations in the application of Equation (5-43). First, those equations apply only to conditions of neutral atmospheric stability—i.e., when the actual temperature gradient in the air near the surface equals the adiabatic lapse rate (Section D.6.8). If the gradient is steeper than adiabatic, turbulent exchange will be enhanced by buoyant forces (unstable conditions); if it is less steep than adiabatic, turbulent exchange will be suppressed (stable conditions). (See Figure D-12.) Stable conditions are common over snowpacks, with temperature not uncommonly *increasing* with elevation (a "temperature inversion"). For these conditions, Equation (5-43) is divided by **stability-correction factors** Φ_M and Φ_H, as in Equation (D-54). These factors are computed via Equation (D-55) and Table D-5.

The second consideration in applying Equation (5-43) is that wind speeds are virtually always measured in fields or clearings, and such measurements must be adjusted for calculating turbulent exchange in forested areas. Few data are available on which to base an adjustment factor; Dunne and Leopold (1978) suggested the following:

$$v_{aF} = (1 - 0.8 \cdot F) \cdot v_{aO}. \quad \textbf{(5-44)}$$

Here, F is the fractional forest cover, and the subscripts F and O indicate wind speed inside and outside of the forest, respectively.

EXAMPLE 5-7

Calculate the average daily turbulent sensible-heat exchange for the conditions given in Examples 5-5 and 5-6. The average wind speed measured in the open, v_{aO}, is 6.00 m s^{-1}; the measurement height, z_a, is 2.00 m.

Solution In the absence of other information, we assume $z_0 = 0.0015$ m; thus Equation (5-43b) can be used directly. Since the site of interest is forested with $F = 0.80$, we apply Equation (5-44) to adjust the wind speed:

$$v_{aF} = (1 - 0.8 \times 0.80) \times 6.00 \text{ m s}^{-1} = 2.16 \text{ m s}^{-1}.$$

Direct use of Equation (5-43b) yields

$$H = 0.348 \times 2.16 \text{ m s}^{-1} \times (4°\text{C} - 0°\text{C}) = 3.01 \text{ MJ m}^{-2} \text{ day}^{-1}.$$

To compute the stability-correction factors, we first calculate the Richardson number, *Ri*, via Equation (D-55):

$$Ri = \frac{2 \times 9.81 \times (2 - 0.0015) \times (4 - 0)}{(277.2 + 273.2) \times (2.16 - 0)^2} = 0.061.$$

As expected, $Ri > 0$, reflecting a stable condition. From Table D-5, we calculate the stability-correction factors:

$$\Phi_H = \Phi_M = (1 - 5.2 \times 0.061)^{-1} = 1.47.$$

Dividing the original value of H by Φ_H and Φ_M then gives the stability-adjusted value:

$$H = \frac{3.01 \text{ MJ m}^{-2} \text{ day}^{-1}}{1.47 \times 1.47} = 1.40 \text{ MJ m}^{-2} \text{ day}^{-1}.$$

Thus the stable atmospheric conditions significantly suppress turbulent transfer.

Turbulent Exchange of Latent Heat with the Atmosphere Latent-heat exchange with the atmosphere is governed by the same turbulent process that produces sensible-heat exchange; this process is described in Section D.6 and leads to Equation (D-42):

$$LE = -\lambda_v \cdot \frac{0.622 \cdot \rho_a}{P} \cdot \frac{k^2}{\left[\ln\left(\frac{z_a - z_d}{z_0}\right)\right]^2} \cdot v_a \cdot (e_a - e_s). \quad \textbf{(D-42)}$$

In this equation, λ_v is the latent heat of vaporization, P is the atmospheric pressure, e_a is the air vapor pressure, e_s is the surface vapor pressure, and the other symbols are as given previously for Equation (D-42).

If the vapor-pressure gradient is directed upward ($e_s > e_a$), water substance will move from the snow to the air (evaporation); if it is directed downward ($e_s < e_a$), water substance will move from the air to the snow (condensation). In applying this equation to snow, however, we note that *two* phase

changes may be involved. For cold snowpacks ($T_{ss} < 0$ °C), evaporation and condensation involve the solid–vapor or vapor–solid phase change (sublimation); then the latent heat involved is the sum of the latent heats of vaporization, λ_v, and fusion, λ_f. For melting snowpacks ($T_{ss} = 0$ °C), no solid–liquid or liquid–solid phase change occurs and only λ_v is involved (Anderson 1968).

To put Equation (D-42) into a form directly applicable to the snow-surface energy balance, we again drop the minus sign, so that energy inputs to the snowpack are positive, and make assumptions analogous to those used in developing Equation (5-43): $\lambda_v = 2.47$ MJ kg^{-1}, $\lambda_f = 0.334$ MJ kg^{-1}, $k = 0.4$, $z_a = 2.00$ m, $z_0 = 0.0015$ m, $P = 101.1$ kPa, and $\rho_a = 1.29$ kg m^{-3}. With these assumptions, we arrive at the following equations:

cold snow ($T_{ss} < 0$ °C)

$$LE = (6.86 \times 10^{-5}) \cdot v_a \cdot (e_a - e_{ss}) \text{ MJ m}^{-2} \text{ s}^{-1}, \quad \textbf{(5-45a)}$$

$$LE = 5.93 \cdot v_a \cdot (e_a - e_{ss}) \text{ MJ m}^{-2} \text{ day}^{-1}; \quad \textbf{(5-45b)}$$

melting snow ($T_{ss} = 0$ °C)

$$LE = (6.05 \times 10^{-5}) \cdot v_a \cdot (e_a - e_{ss}) \text{ MJ m}^{-2} \text{ s}^{-1}, \quad \textbf{(5-46a)}$$

$$LE = 5.22 \cdot v_a \cdot (e_a - e_{ss}) \text{ MJ m}^{-2} \text{ day}^{-1}. \quad \textbf{(5-46b)}$$

In these equations, v_a is in m s^{-1} and vapor pressures are in kPa.

As with the turbulent exchange of sensible heat, Equation (5-44) may be appropriate for estimating wind speeds in forests, and stability effects may be accounted for by using the approach described in Section D.6.8 and Example 5-7.

EXAMPLE 5-8

Compute the turbulent exchange of latent heat for the conditions given in Example 5-7.

Solution We first decide whether evaporation or condensation is occurring by comparing e_a and e_{ss}. The snow is at 0 °C, so $e_{ss} = 0.611$ kPa. In Example 5-6, we found that $e_a = 0.651$ kPa; since $e_a > e_{ss}$, we have condensation on melting snow and Equation (5-46b) is applicable. The appropriate value of wind speed is as found in Example 5-7: $v_a = 2.16$ m s^{-1}. Thus

$$LE = 5.22 \times 2.16 \text{ m s}^{-1} \times (0.651 \text{ kPa} - 0.611 \text{ kPa}) = 0.451 \text{ MJ m}^{-2} \text{ day}^{-1}.$$

As in Example 5-7, this value must be adjusted by the stability factors, giving

$$LE = \frac{0.451 \text{ MJ m}^{-2} \text{ day}^{-1}}{1.47 \times 1.47} = 0.210 \text{ MJ m}^{-2} \text{ day}^{-1}.$$

Various studies have found significantly different values for the "constants" in the turbulent-exchange equations. [See, for example, Male and Gray (1981).] This variability may be due to differences in (1) the periods over which measurements are averaged, (2) measurement heights, (3) roughness heights, (4) the ways in which stability effects are accounted for, or (5) the degree to which the assumed wind profiles coincide with actual conditions. Because of these factors, one must recognize that energy-budget values calculated with these equations are approximate.

In forests, snow evaporation occurs from the snow intercepted on the canopy, and evaporation from the ground becomes important only after the intercepted snow has disappeared by ablation or falling or blowing off (Lundberg and Halldin 1994). There is evidence that evaporation of intercepted snow may occur at rates of up to 3.3 mm day^{-1} and may be an important component of the snow ablation in forests—perhaps amounting to 200 mm or more per winter (Lundberg et al. 1997).

Heat Input by Rain When rain falls on a snowpack that is at the freezing point ($T_s = T_m$), the rainwater is cooled to the snow temperature and the heat given up by the water is used in melting. Thus for this situation, we can calculate the heat contributed by rain, R, as

$$R = \rho_w \cdot c_w \cdot r \cdot (T_r - T_m), \quad \textbf{(5-47a)}$$

where c_w is heat capacity of water (4.19×10^{-3} MJ kg^{-1} K^{-1}), r is the rainfall rate [L T^{-1}], and T_r is the temperature of the rain.

When rain falls on snow that is below freezing, it will first cool to the freezing point, giving up sensible heat according to Equation (5-47a), and then freeze, liberating latent heat. In this case we have

$$R = \rho_w \cdot c_w \cdot r \cdot (T_r - T_m) + \rho_w \cdot \lambda_f \cdot r. \quad \textbf{(5-47b)}$$

If humidity information as well as the air temperature is available, T_r can be estimated as the dew-point temperature, which is given by Equation

(D-11). However, since relative humidity usually is close to 1 during rain, and since R is rarely a large contributor to the energy balance, the usual practice is to assume $T_r = T_a$.

EXAMPLE 5-9

Compute the heat contributed by 25 mm of rain falling on the snowpack considered in the previous examples.

Solution Since the snow is at 0 °C, Equation (5-47a) is applicable. We assume that $T_r = T_a$ and that interception loss on the forest canopy is negligible. (See Section 7.6.) Thus

$$\begin{aligned} R &= 1000 \text{ kg m}^{-3} \times (4.19 \times 10^{-3} \text{ MJ kg}^{-1} \text{ K}^{-1}) \\ &\quad \times 0.025 \text{ m day}^{-1} \times (4 \text{ °C} - 0 \text{ °C}) \\ &= 0.419 \text{ MJ m}^{-2} \text{ day}^{-1}. \end{aligned}$$

Note that R in this case is relatively large compared with the other energy-balance components computed in Examples 5-5–5-8. This unusual situation arises because the rainfall rate was high and because K, H, and LE are severely reduced on a steeply sloping north-facing slope with a dense forest cover.

Conductive Exchange of Sensible Heat with the Ground Temperatures in the soil under snowpacks usually increase downward due to thermal energy stored during the summer and geothermal heat. Thus, in these circumstances, heat is conducted upward to the base of the snowpack at a rate G given by

$$G = k_G \cdot \frac{dT_G}{dz}, \qquad \textbf{(5-48)}$$

where k_G is the thermal conductivity of the soil [E L^{-1} T^{-1} θ^{-1}], T_G is the soil temperature, and z is the distance below the ground surface.

Thermal conductivities of soils depend on soil texture, soil density, and moisture content and vary widely spatially and temporally. For example, the U.S. Army Corps of Engineers (1956) reported a more than tenfold increase in k_G during the melt season in the soil they studied, from 8.37×10^{-3} to 0.100 MJ m^{-1} K^{-1} day^{-1}. This variability, along with the general lack of information about thermal conductivity and ground-temperature gradients, usually precludes accurate computation of G. This uncertainty has little practical effect on energy-balance estimates during the snowmelt season, however, because G is usually negligible compared with other terms.

In spite of its generally negligible contribution during the melt season, the energy conducted to the snowpack from the ground during the accumulation season can be hydrologically significant. Studies from various localities (Federer and Lash 1978; Male and Gray 1981) indicate that this heat produces continual melting at the base of the snowpack, called **groundmelt,** at rates up to 2 mm day^{-1}. Groundmelt can add significantly to moisture in the soil, increasing the percentage of snowmelt that will run off during the snowmelt season and, in regions like New England, groundmelt may be the principal source of flow in upland streams during the winter.

Case Study of Snowmelt at Danville, VT, USA

The accumulation and melt of a snowpack during a typical winter (1972–1973) at the U.S. National Weather Service–U.S. Agricultural Research Service Snow Research Station in Danville, VT, are traced in Figure 5-24. Although the average snowpack temperature was not measured, the beginnings and ends of the accumulation period and the phases of the melt period can be approximated from the traces of depth, average snowpack density, water equivalent, and average air temperature.

The air temperature was above 0 °C only occasionally between mid-November and late February, and the water equivalent of the pack increased more or less continually during this period due to snowfalls and minor rain. The maximum snow depth of 72 cm was reached in late February. The density was initially about 100 to 150 kg m^{-3}, jumped to about 250 kg m^{-3} in early December, and increased gradually thereafter to about 300 kg m^{-3} when the melt season began. Density increases were due largely to constructive metamorphism and occasionally to refreezing at depth of rain and surface melt.

The accumulation period ended when air temperature began a final rise on 26 February; temperature was above freezing from 4 to 17 March, and water equivalent began to decline on 4 March. Significant water output was measured in a snowmelt lysimeter from 9 through 18 March. Density climbed from about 300 kg m^{-3} to 400 kg m^{-3} during the first two phases of melt; it then fluctuated between 350 and 450 kg m^{-3} and eventually reached 520 kg m^{-3} just before melting was complete.

Table 5-3 gives the amounts of energy involved in each of the components of the energy budget during the accumulation and melt periods for six

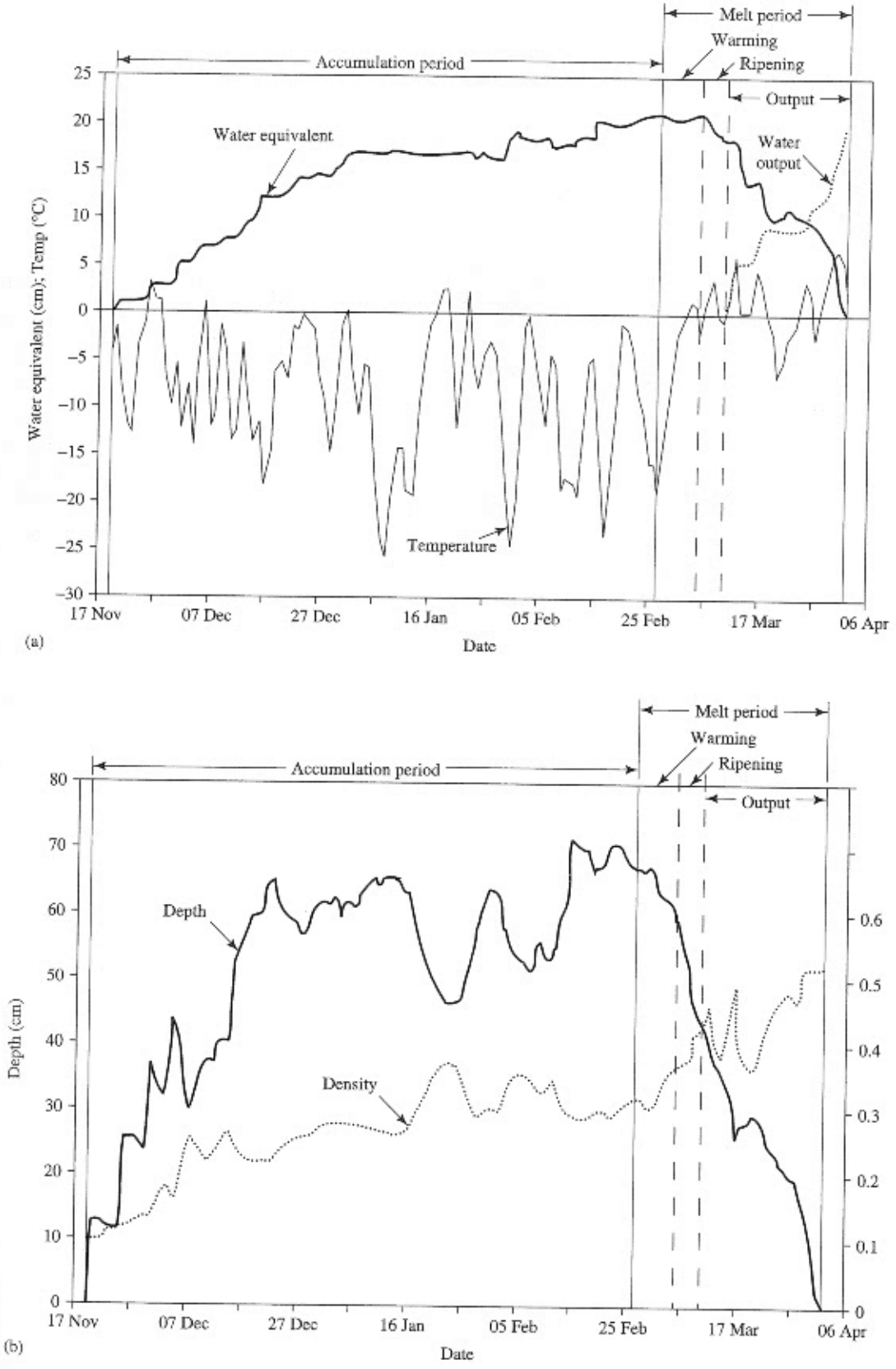

FIGURE 5-24
(a) Snowpack water equivalent, average air temperature, and cumulative water output; and (b) snowpack depth and density at the Sleepers River Research Watershed in Danville, VT, USA, for 1972–1973. The accumulation period and three phases of the melt period are shown; the boundary between the warming and ripening phases is uncertain. Data from Anderson et al. (1977).

TABLE 5-3
Energy-Balance Components (MJ m^{-2}) for Six Seasons at the U.S. National Weather Service–U.S. Agricultural Research Service Snow Research Station, Danville, VT. Data from Anderson (1976).

	68–69	69–70	70–71	71–72	72–73	73–74	Average
				Accumulation Season			
Net shortwave radiation, K	167.94	171.50	195.28	169.70	115.14	191.76	168.55
Net longwave radiation, L	−264.49	−259.64	−282.87	−238.95	−174.39	−225.85	−241.03
Net radiation, $K + L$	−96.55	−88.14	−87.59	−69.25	−59.25	−34.08	−72.48
Heat from rain, R	0.08	0.84	0.25	0.38	0.71	1.00	0.54
Heat from ground, G	30.77	53.89	32.24	25.00	26.29	29.73	32.99
$K + L + R + G$	−65.69	−33.41	−55.10	−43.88	−32.24	−3.35	−38.95
Turbulent exchange, sensible, H	96.76	84.37	112.92	92.49	65.40	81.86	88.97
Turbulent exchange, latent, LE	−11.97	−25.88	−27.13	−24.45	−16.08	−20.39	−20.98
$H + LE$	84.79	58.49	85.79	68.04	49.32	61.47	67.98
Net heat input, S	19.09	25.08	30.69	24.16	17.08	58.12	29.04
				Melt Season			
Net shortwave radiation, K	191.97	129.00	162.83	150.73	149.69	168.78	158.83
Net longwave radiation, L	−101.12	−67.49	−77.29	−74.78	−92.45	−109.99	−87.19
Net radiation, $K + L$	90.86	61.51	85.54	75.95	57.24	58.79	71.65
Heat from rain, R	0.46	0.63	0.71	1.26	0.67	1.17	0.82
Heat from ground, G	5.23	3.56	5.07	4.27	9.55	9.30	6.16
$K + L + R + G$	96.55	65.69	91.32	81.48	67.45	69.25	78.62
Turbulent exchange, sensible, H	66.57	43.13	67.12	65.86	56.32	60.80	59.96
Turbulent exchange, latent, LE	−28.35	−17.88	−23.66	−28.85	−35.00	−31.90	−27.61
$H + LE$	38.23	25.25	43.46	37.01	21.31	28.89	32.36
Net heat input, S	134.78	90.94	134.78	118.49	88.76	98.14	110.98

seasons at the Danville site. For all accumulation seasons, L was negative and more than balanced K, resulting in negative net radiation. H was positive and LE negative in all accumulation seasons, but the magnitude of H was several times greater than that of LE, so there was a net input of heat from turbulent exchange. There was a very small contribution from rain. The overall positive net input is largely due to ground heat, which was sufficient to produce about 87 mm of groundmelt.

In all melt seasons, the input from K was about twice the loss via L, resulting in a strongly positive net radiation. Energy input was augmented slightly by G and negligibly by R. Again, sensible-heat exchange was positive, and latent-heat exchange was negative but of considerably smaller magnitude, giving a net input from turbulent-exchange processes. The positive net heat input for melt seasons is the energy used in melting.

Comparison of Energy Balances in Different Environments

Kuusisto (1986) reviewed over 20 studies of melt-period energy balances; his summary is given in Table 5-4. The comparable information for Anderson's (1976) study (computed for the melt season from Table 5-3) has also been added to Table 5-4. Kuusisto (1986) made the following generalizations based on his survey:

- Net radiation and turbulent exchange play a major role in the energy balance, and heat from rain and from the ground are small or negligible.
- Net radiation and sensible-heat exchange are positive during snowmelt in most locations.
- Latent-heat exchange is positive in some places, but negative in others.
- The net radiation is the most important component in forests, probably due to the reduced wind speeds.
- On cloudy or rainy days, turbulent heat exchange dominates.
- Very high areal snowmelt rates are usually caused by intense positive turbulent heat exchange.

The last generalization has implications for forecasting conditions that can cause snowmelt flooding: very warm, humid air and high winds

TABLE 5-4
Relative Contributions of Energy-Balance Components to Snowmelt in Different Environments[a]

Study	Site[b]	Period[c]	Percent Contribution from				
			K + L	*H*	*LE*	*R*	*G*
1	Open field, CA, 37°N		72	28	–18		
2	Open field, Canada, 45°N (100 m)	Mar 59 (0.7)	75	25	–74		
3	Open field, AK, 67°N	Mar–Apr 66	86	14	24		
4	Open field in mts., CA, 37°N	Apr–May 47–51 (daytime)	73	23	4		
5	Open field, MI, 46°N	23 Jan 69 (1.5)	17	47	36		
6	Forest opening, CO, 39°N (3260 m)	Jun 68 (5.0)	56	44	–3	0	
7	Open field in mts., France, 46°N (3550 m)	Jul 68 (1.6)	85	15	–15		
8	Open field in mts., Spain, 41°N (1860 m)	Apr 70 (1.0)	100	–11	–42		
9	Open field, AK, 71°N (10 m)	Jun 71	100	–19	–10		–22
10	Open field in prairie, Canada, 51°N	Melt season 74 (0.8)	59	41	–10		–6
11	Open field in prairie, Canada, 51°N	Melt season 75 (0.5)	95	5	–29		–1
12	Open field in prairie, Canada, 51°N	Melt season 76 (0.3)	67	33	–14		–4
13	Deciduous forest, Ontario, 46°N	Apr 78 (1.0)	100	0	0		
14	Open field, Finland (60 m)	Melt seasons 68–73 (0.7)	46	53	–4	1	
15	Open field in mts., Norway, 60°N	Apr–May 79–80 (1.2)	35	65	0		
		cloudy days (2.3)	20	54	26		
		clear days (0.7)	37	63	–24		
16	Small basin, 23% forest, Switzerland, 47°N (800 m)	Days with intense snowmelt, 77–80 (2.3)	8	65	20	7	
17	Open field, AK, 65°N	Apr 80 (0.3)	67	33	–68		0
18	Open field, Finland, 61°N	Days with intense snowmelt, 59–78 (1.4)	48	47	2	3	
19	Open field, Finland, 67°N	Days with intense snowmelt, 59–78 (1.5)	58	40	–23	2	
20	Open tundra, N.W.T., Canada, 79°N (200 m)	Melt seasons 69–70	100	–90	–77		–45
21	Open field in mts., New Zealand, 43°S (1500 m)	Oct–Nov 76–80	30	57	13	<1	
		Rainy days	17	55	25	3	
		Days with greatest heat input	16	60	23	1	
22	Open field in mts., New Zealand, 43°S (1450 m)	Melt season 82 (3.1)	16	57	25	2	
23	Open field, WI, 3 sites, 43–45°N	Melt seasons 53–64	–31	100	–12		
24	Small basin, 82% forest, Finland 64°N (120 m)	Melt seasons 71–81 (0.5)	86	14	–13	<1	
25	Open field, hilly area, VT, 45°N (550 m)	Melt seasons 69–74 (1.3)	52	43	–20	<1	4

[a]100% is the sum of all positive components. Data from Kuusisto (1986): see that paper for references to individual studies. Data from Anderson (1976) added as study 25.

[b]Number in parentheses is site elevation.

[c]Number in parentheses is average melt in cm day^{-1}.

above a ripe snowpack. The potential for flooding under these conditions is increased because this situation would typically exist generally over a watershed, whereas rapid melting due to solar radiation is restricted largely to south-facing nonforested slopes. When rain accompanies warm winds, the flooding potential may be further exacerbated by the rain to produce a "rain-on-snow event," such as the one that generated the record floods of March 1936 in central New England. Note that the heat introduced by the rain plays only a small role in generating melt; in some cases the rain itself, with little melt, can produce floods (Singh et al. 1997).

5.4.3 Movement of Water through Snow

Percolation and Water-Output Production

We saw earlier that a ripe snowpack typically retains only a small fraction of its water equivalent as liquid water, which is present as thin films held by surface tension occupying less than 10% of the pore space (Figures 5-19 and 5-20). As additional water is produced during the last phase of melting, the water can no longer be held against gravity and downward percolation begins. Natural snowpacks are seldom homogeneous and usually contain discontinuous layers of varying density that temporarily store and horizontally divert the percolating water (Marsh and Woo 1985; Conway and Benedict 1994). However, ice layers disappear rapidly as melt progresses, and melting snowpacks tend to become fairly uniform assemblages of semi-spherical grains of from 1 to 3 mm in diameter. Thus to gain a basic understanding of the physical processes involved, it is appropriate to treat melting snowpacks as **homogeneous porous media,** physically identical to coarse-grained soils.

As noted, the pores of snowpacks are only partially filled with liquid water.[7] Thus the vertical percolation of water in the snowpack is a form of **unsaturated porous-media flow,** which is discussed in detail in Section 6.3 and Box 6-1. Colbeck (1978) gave a detailed description and experimental validation of the application of these relations to snowmelt percolation. He showed that capillary forces in snow are usually negligible in relation to gravitational forces, so the equation of motion [Darcy's Law, Equation (6B1-6)] can be simplified to

$$V_{z'} = K_h(\theta_w), \tag{5-49}$$

where $V_{z'}$ is the vertical flux rate (volume of water per unit horizontal area) and K_h is the hydraulic conductivity of the snow. As for soils, K_h is a function of the liquid–water content, θ_w, which can be represented as

$$K_h(\theta_w) = K_h^* \cdot \left(\frac{\theta_w - \theta_{ret}}{\phi - \theta_{ret}}\right)^c, \tag{5-50}$$

where K_h^* is the hydraulic conductivity for completely saturated snow and c is an empirical exponent with a value $c = 3$.[8] K_h^*, in turn, is a function of snow density:

$$K_h^* = 0.0602 \cdot \exp(-0.00957 \cdot \rho_s), \tag{5-51}$$

where K_h^* is in m s^{-1} and ρ_s is in kg m^{-3} (Sommerfield and Rocchio 1993).

Energy inputs to the surface of a ripe snowpack vary diurnally, usually approximating a sine curve with a peak input in the early afternoon. This variation generates a daily wave of meltwater originating near the surface and percolating downward (Figure 5-25). As discussed by Dunne et al. (1976) and Colbeck (1978), the rate of travel, U_z, of a wave is related to the snow properties and flux rate, $V_{z'}$, as

$$U_z = \frac{c}{\phi - \theta_{ret}} \cdot K_h^{*1/c} \cdot V_{z'}^{(c-1)/c}. \tag{5-52}$$

Because the speed of these melt waves increases as the flux (melt) rate increases, water produced during the period of peak melting near midday overtakes water produced earlier in the day. Thus the waves tend to accumulate water and develop a sharp wave front, as in Figures 5-25 and 5-26.

Example 5-10 shows how Equation (5-52) can be used to estimate the time of travel of a melt wave through a snowpack and how Equations (5-50) and (5-51) can be used to estimate the liquid-water content of a melting snowpack.

[7] This discussion applies to snowpacks above any basal saturated zone that may form where meltwater accumulates at an ice layer or at the ground surface.

[8] Equation (5-50) is analogous to Equation (6-13b).

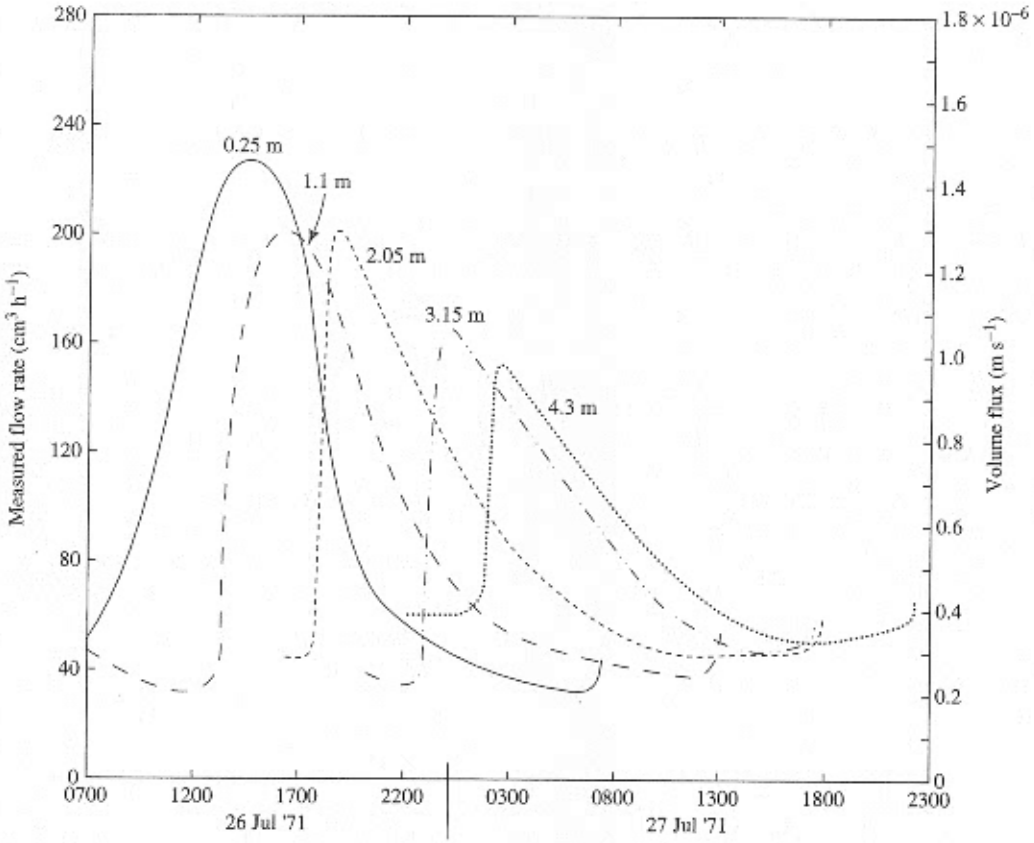

FIGURE 5-25
Volume rates of flow at different depths in a homogeneous snowpack produced by a day of intense fair-weather melting. From Colbeck (1978).

EXAMPLE 5-10

Compute (a) the time lag of water output and (b) the liquid-water content for the snowpack considered in Examples 5-5–5-9.

Solution (a) If groundmelt is negligible, the total energy input for the day considered, S, is

$$S = K + L + H + LE + R = 0.19 + 0.27 + 1.40 + 0.21 + 0.42 = 2.49 \text{ MJ m}^{-2} \text{ day}^{-1}.$$

The melt rate is found via Equation (5-24) as

$$h_m = \frac{2.49 \text{ MJ m}^{-2} \text{ day}^{-1}}{1000 \text{ kg m}^{-3} \times 0.334 \text{ MJ kg}^{-1}} = 0.00746 \text{ m day}^{-1} = 7.5 \text{ mm day}^{-1}.$$

Adding to this result the 25-mm rain, the total water output is 32.5 mm $\text{day}^{-1} = 3.76 \times 10^{-7}$ m s^{-1}. This value is the flux rate $V_{z'}$, in Equations (5-49) and (5-52). Using the density $\rho_s = 400$ kg m^{-3}, we find from Figure 5-20 that $\phi = 0.58$ and $\theta_{ret} = 0.013$ and compute

$$K_h^* = 0.0602 \cdot \exp(-0.00957 \cdot 400) = 1.31 \times 10^{-3} \text{ m s}^{-1}$$

from Equation (5-51). Inserting these values into Equation (5-52) and taking $c = 3$ yields

$$U_z = \frac{3}{0.58 - 0.013} \times (1.31 \times 10^{-3} \text{ m s}^{-1})^{1/3} \times (3.76 \times 10^{-7} \text{ m s}^{-1})^{2/3} = 3.02 \times 10^{-5} \text{ m s}^{-1} = 2.61 \text{ m day}^{-1} = 0.11 \text{ m hr}^{-1}.$$

If the snow depth is 0.725 m, it will take 6.7 hr for the meltwater wave to travel through the snowpack.

(b) To find the water content associated with this melt wave, note that Equations (5-49) and (5-50) can be combined and solved for θ:

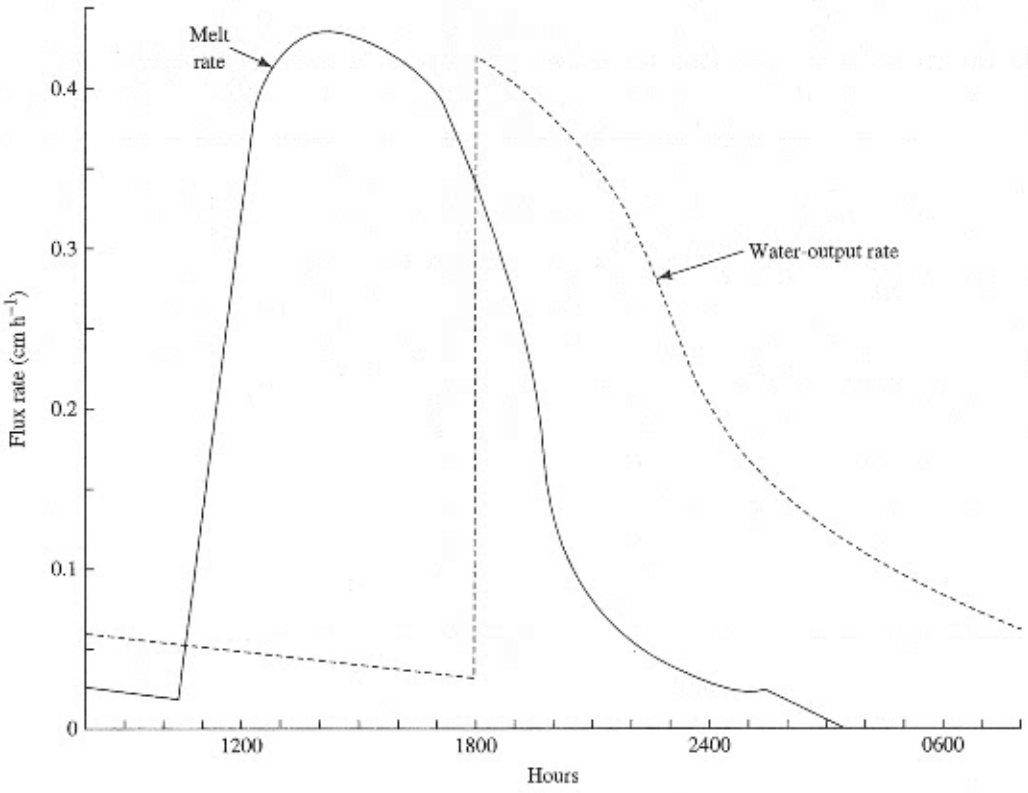

FIGURE 5-26
Comparison of timing of the rate of melting at the surface (the "input") and the rate of vertical unsaturated flow (water output) at the base of a 101-cm-deep tundra snowpack. From Dunne et al. (1976); used with permission of the American Geophysical Union.

$$\theta = (\phi - \theta_{ret}) \cdot \left(\frac{V_{z'}}{K_b^*}\right)^{1/c} + \theta_{ret}$$

Thus

$$\theta = (0.58 - 0.013) \times \left(\frac{3.76 \times 10^{-7}\ \text{m s}^{-1}}{1.31 \times 10^{-3}\ \text{m s}^{-1}}\right)^{1/3} + 0.013 = 0.05.$$

One can calculate that the peak of the wave in Figure 5-25 moves at a velocity of 0.2 to 0.3 m hr^{-1}, which is in the general range found in Example 5-10 and in other studies (Figure 5-27). Thus for most seasonal snowpacks, the peak water output will occur within a few hours of the peak melt rate.

Anderson (1973) developed an empirical expression for the **time lag** of snow melt, i.e., the elapsed time between the beginning of daily melt and the beginning of water output. This expression was designed for use with a model using a 6-hr time step and is given by

$$t_{lag} = 5.33 \cdot \left[1.00 - \exp\left(-\frac{0.03 \cdot h_m}{\Delta h_{w6}}\right)\right], \quad \textbf{(5-53)}$$

where t_{lag} is the time lag (hr), h_m is the water equivalent of the snowpack when melt begins (m), and Δh_{w6} is the amount of melt generated in a 6-hr period (m).

Snowmelt-Runoff Generation

Water arriving at the bottom of the snowpack infiltrates into the soil and/or accumulates to form a saturated zone at the base of the snowpack, moving toward a surface-water body by one of the paths illustrated in Figure 5-28. In case (a) of that figure, the water table is at depth, the ground surface is unsaturated, and all of the water output infiltrates and moves streamward as subsurface flow. In case (b), the surface cannot accept all the water output, and a basal saturated zone develops within the snowpack through which water flows toward the stream.

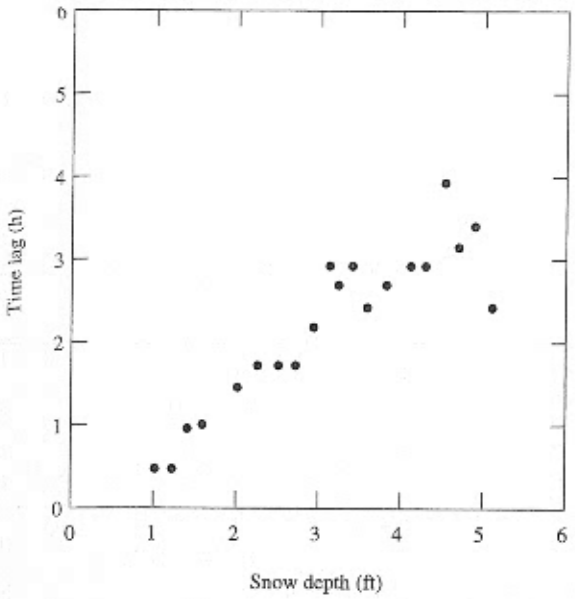

FIGURE 5-27
Approximate time lag between the time of peak surface melting and the time of peak flow from the bottom of a snowpack as a function of snow depth. From Anderson (1968); used with permission of the American Geophysical Union.

In case (c), the ground conditions are similar to those of case (a), but the water table has risen above the ground surface on the lower part of the slope, so that water moves streamward by both surface and subsurface routes.

The process of infiltration is discussed in detail in Chapter 6, and runoff generation by processes similar to those shown in Figure 5-28 is examined in Section 9.2. For now, we explore aspects of snowmelt-runoff generation by the process shown in Figure 5-28b. Assuming a constant snow depth, the daily wave of water output arrives at the base of the snowpack at the same time all along the slope. This input produces daily waves that travel downslope in the basal saturated zone at a velocity, U_s, where

$$U_s = \frac{K_h^*}{\phi - \theta_{ret}} \cdot S_s, \qquad \textbf{(5-54)}$$

In this equation, K_h^* is the saturated hydraulic conductivity, ϕ is the porosity of the basal snow layer, and S_s is the tangent of the slope angle.

As for percolation, K_h^* can be estimated from the snow density via Equation (5-51). However, because of more rapid metamorphism in the saturated zone, the size of snow grains can be significantly larger there than in the unsaturated zone. For example, for a subarctic snowpack, Dunne et al. (1976) found $d = 6$ mm in the basal saturated zone and $d = 2$ mm in the unsaturated zone. Thus, Equation (5-51) may significantly underestimate K_h^* in the basal saturated zone.

Using the wave velocity U_s, one can calculate the average time of travel of water in the basal saturated zone, t_s, as

$$t_s = \frac{L}{2 \cdot U_s}, \qquad \textbf{(5-55)}$$

where L is the slope length. t_s is typically on the order of 1% of the travel time through the unsaturated zone (Male and Gray 1981). Thus, where a basal saturated zone forms, the lag time between peak melt rates and peak inputs to small upland streams is determined largely by the travel time associated with the vertical percolation through the snowpack and is typically on the order of several hours. In contrast, infiltrating snowmelt that percolates through the soil to the ground water (Figure 5-28a) may not appear in streamflow for months (Bengtsson 1988).

Singh et al. (1997) developed a model for the flow of water in a basal saturated zone; we will explore the phenomenon further in Section 9.2.3.

5.5 SNOWMELT MODELING

5.5.1 Snowmelt at a Point

Energy-Balance Approach

The energy-balance relations given by Equations (5-18)–(5-48) form the basis for one class of models of snowmelt at a point. These models are described as "physically based," because the energy balance is a fundamental physical principle (conservation of energy) and because they use equations that describe the physics of processes in each component of the energy balance. The general logic of a typical energy-balance model is diagrammed in Figure 5-29.

Much of the discussion in this section is based on the work of Anderson (1976), as this work appears to be the most thorough and extensive study

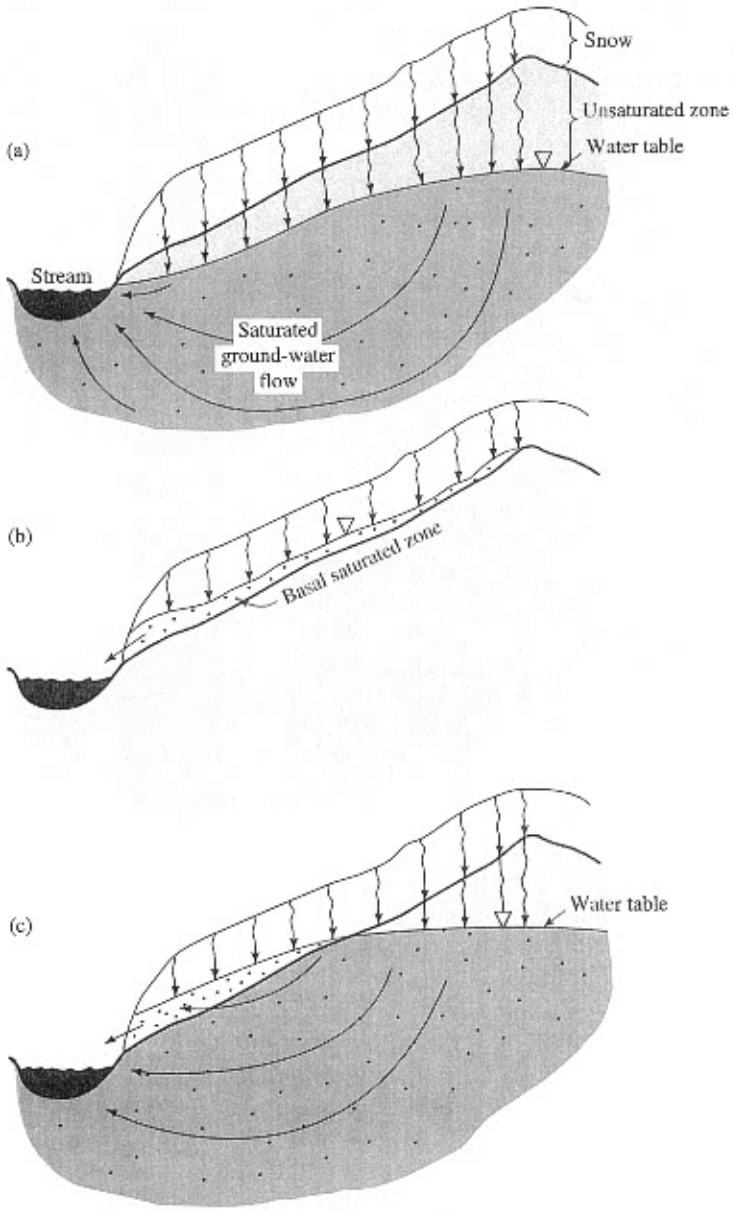

FIGURE 5-28
Three modes of snowmelt-runoff generation. (a) The top of the saturated zone in the soil (water table) is at depth; percolating meltwater infiltrates and percolates to the saturated zone to raise the water table and thereby induce increased ground-water flow to the stream. (b) The water table is at the soil surface, or the soil surface is impermeable (perhaps due to solid soil frost); percolating meltwater accumulates to form a basal saturated zone through which water drains to the stream. (c) The lower portion of the water table has risen above the ground surface into the snowpack; water in the upper part of the slope moves as in (a), and water in the lower part moves as in (b). Modified after Dunne and Leopold (1978).

and testing of point snowmelt-modeling techniques. Anderson's studies were conducted in a large clearing at an elevation of 550 m in Danville, VT, over a period of six years. Energy-balance modeling of snowmelt under a forest cover has not been carefully tested.

Time Step In order to develop a computer model based on Equation (5-18), one must first decide on the time step, Δt, to be used. Anderson (1976) compared results using $\Delta t = 1, 3$, and 6 hr and found only minor differences.

Time periods of up to 24 hr will probably give reasonably satisfactory results, because the energy-balance components are linear or nearly linear functions of the meteorologic and other independent variables [Equations (5-27)–(5-48)]. Linearity guarantees that

$$E_i\{f[x(t)]\} = f[E_i\{x(t)\}], \tag{5-56}$$

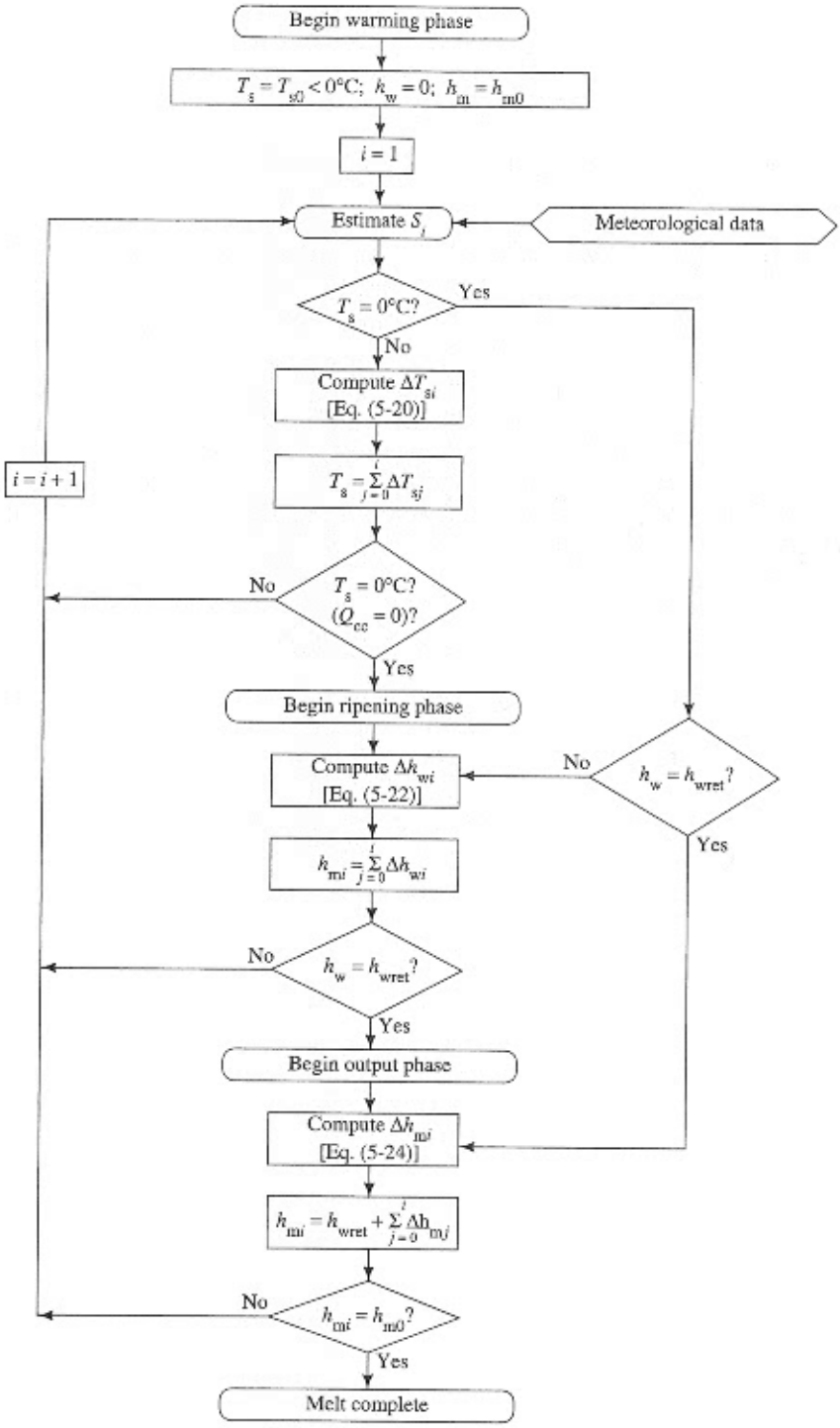

FIGURE 5-29
Flowchart showing how the energy balance is used in modeling snowmelt. The subscript i is the counter for successive time periods of length Δt.

where $E_t\{\ \}$ indicates a time average, $f[\ ]$ is a linear function, and $x(t)$ represents one or more independent variables that are functions of time.

Potential exceptions to this near linearity are in the turbulent-exchange equations, where wind speed is multiplied by another variable; distortions due to time averaging for these equations will occur in proportion to the degree of independent variation of the variables involved. Even though Equation (5-37) appears highly nonlinear, the relation is nearly linear over the range of temperatures encountered.

Layer Thickness Water and energy move vertically in a snowpack, so development of a snowmelt model also requires a decision about the thickness of the layers within the snowpack to be represented in the model. Anderson (1976) compared results using thicknesses of 1, 2.5, 5, and 10 cm, and found that the predicted water equivalent at a given time increased as the thickness increased because the thicker layers introduced distortions in the diurnal warming–cooling cycles. Although there is little further evidence on which to base definitive guidelines, one could probably expect significant distortions to appear in energy-balance models using thicknesses exceeding 50 to 100 cm. However, many models, including the BROOK90 model introduced in Section 2.9.5, treat the snowpack as a single layer of varying depth.

Data Requirements Clearly, use of the energy-balance approach requires measurement of a large number of variables, including at least air temperature, humidity, wind speed, cloud cover, precipitation, snow-surface temperature, and, ideally, incident and outgoing short- and longwave radiation. Measurements of these variables must be made at representative locations and with sufficient frequency to calculate at-least-daily averages.

Validation The soundness of any model must be established by "validation"—that is, by comparing its forecasts with actual events that were not used in developing the model. (See Section 2.9.4.) Anderson (1976) compared snowmelt and water equivalent estimated by the energy-balance model with those measured at the intensively instrumented Danville site. These comparisons are presented following discussion of the temperature-index approach to snowmelt modeling in the next section.

Temperature-Index Approach

Because of the difficulty and expense of fulfilling the data requirements of the energy-balance approach—and, in fact, the virtual impossibility of collecting such data at enough locations to be spatially representative of even a moderate-sized watershed—the empirical **temperature-index approach** is incorporated in most models used to predict or forecast snowmelt runoff. This approach estimates snowmelt, Δw, for a daily or longer time period as a linear function of average air temperature:

$$\begin{aligned} \Delta w &= M \cdot (T_a - T_m), & T_a \geq T_m; \\ \Delta w &= 0, & T_a < T_m. \end{aligned} \quad \textbf{(5-57)}$$

Here, M is called a **melt coefficient, melt factor,** or **degree-day factor.**

The logic of this approach is clear when one recognizes that, during melting, the snow-surface temperature is at or near 0 °C, that energy inputs from longwave radiation and turbulent exchange are approximately linear functions of air temperature, and that there is a general correlation between solar radiation and air temperature. Figure 5-30 shows that a relation like Equation (5-57) reasonably approximates daily melt at the Danville snow-research site—although there is considerable scatter. The value of M that best fits these data is M = 3.6 mm day^{-1} °C^{-1}, and the intercept value, –1.4 mm day^{-1}, is not significantly different from 0.

However, the value of M varies with latitude, elevation, slope inclination and aspect, forest cover, and time of year and ideally should be empirically estimated for a given watershed. Male and Gray (1981) cited a study suggesting that, in the absence of site-specific data, M can be estimated as

$$M = 4.0 \cdot (1 - a) \cdot \exp(-4 \cdot F) \cdot f_{sl}, \quad \textbf{(5-58)}$$

where M is in mm day^{-1} °C^{-1}, a is albedo (see Figure 5-23), F is the fraction of forest cover, and f_{sl} is the **slope factor,** i.e., the ratio of solar radiation received on the site of interest to that on a horizontal surface [Equation (E-27), a function of latitude, day of year, slope inclination, and slope aspect]. Federer and Lash (1978) expressed the melt factor for forests in the eastern United States as

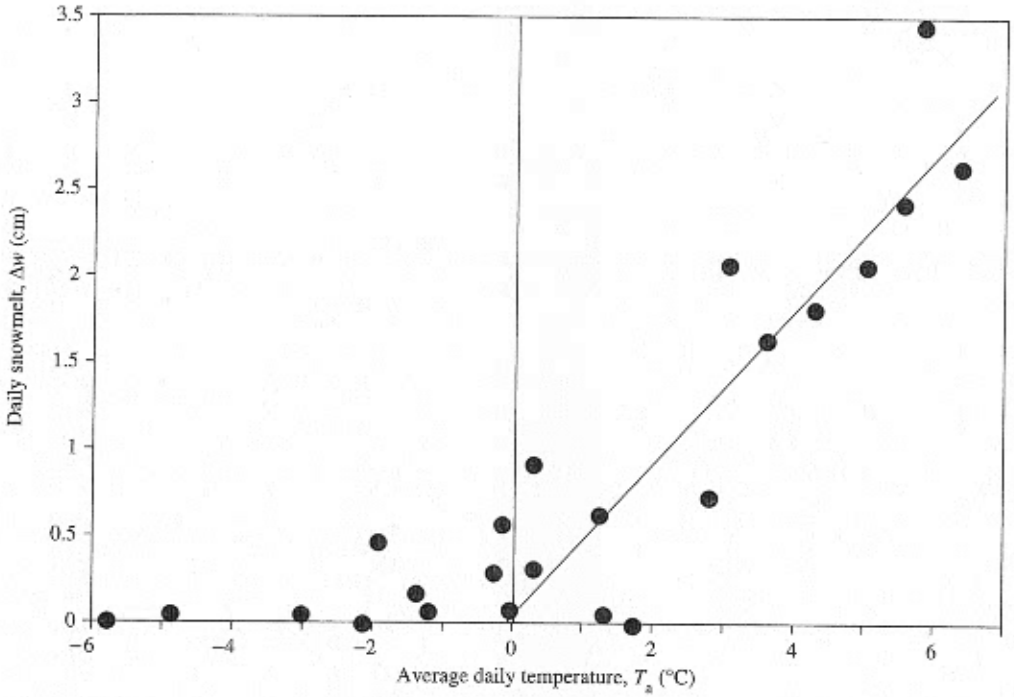

FIGURE 5-30
Daily snowmelt, Δw, as a function of daily average air temperature, T_a, at Danville, VT, in March 1973. The line is the best-fit linear relation between the two variables for days when $T_a > 0$ °C. Data from Anderson et al. (1977).

$$M = f_F \cdot (0.7 + 0.0088 \cdot J) \cdot f_{sl}, \quad J < 183, \qquad \textbf{(5-59)}$$

where f_F is a vegetative-cover factor equal to 30.0 for open areas, 17.5 for hardwood forests, and 10.0 for conifer forests, and the other symbols are as in Equation (5-58).

Kuusisto (1980) recommended relating M to density, which generally increases during the melt season. For the forest,

$$M = 10.4 \cdot \frac{\rho_s}{\rho_w} - 0.7; \qquad \textbf{(5-60a)}$$

in the open,

$$M = 19.6 \cdot \frac{\rho_s}{\rho_w} - 2.39. \qquad \textbf{(5-60b)}$$

In both equations, M is in mm day^{-1} °C^{-1}.

Further adjustments in M must be made to account for differences in the value of air temperature at the measurement site and the value applicable to the area being modeled.

Hybrid Approach

The variability in melt factor as a function of time of year, land cover, and slope factor largely reflects the importance of solar radiation on snowmelt. To reduce this variability and improve prediction accuracy while retaining practical data requirements, Kustas et al. (1994) and Brubaker et al. (1996) evaluated an approach that computes daily snowmelt, Δw, as

$$\Delta w = \frac{K + L}{\rho_w \cdot \lambda_f} + M_r \cdot T_a, \qquad \textbf{(5-61)}$$

where M_r is a "restricted" melt factor with a constant value of 2.0 mm day^{-1} °C^{-1}. In this method, the radiation terms are measured or evaluated via Equations (5-29)–(5-42), and M_r accounts for the turbulent-exchange processes. Brubaker et al. (1996) showed that the value of $M_r = 2.0$ mm day^{-1} °C^{-1} can be derived from the basic equations for those processes [Equations (D-46) and (D-47)].

Evaluation of Point Snowmelt Models

The report by Anderson (1976) covering six snow seasons at Danville, VT, is the most thorough comparison of point energy-balance and temperature-index modeling with actual data. Anderson's complete model included simulation of snowpack settling and compaction as well as the snowpack energy balance and was used for both accumulation and melt seasons. The temperature-index model, calibrated for the Danville site, is applicable only for the output phase of the melt seasons.

Figure 5-31 compares snow-course measurements of snowpack water equivalent and density with values simulated by Anderson's complete energy-balance model for the accumulation season and the warming and ripening phases of the melt season in 1972–1973. Figure 5-32 shows the same comparison for the output phase and includes the predictions of the temperature-index model. Computed daily water output is compared with values measured in a lysimeter in Figure 5-33.

Clearly, both models perform very well in simulating density and water equivalent for the 1972–1973 snow season; this is also the case for 1971–1972. In three of the other melt seasons examined, the energy-balance model gave somewhat better results, while the temperature-index model was slightly better during one season. Except for two of the highest output days, predictions of water output were also good.

Figure 5-34 compares lysimeter-measured snowmelt with melt estimated via a complete energy-balance approach, the temperature-index approach with seasonally increasing melt coefficient, and the hybrid approach with radiation terms estimated as in Equations (5-29)–(5-42). The accuracy of the hybrid approach was almost identical to that of the complete energy-balance approach, and both methods performed considerably better than the temperature-index approach.

These results lead to the following conclusions:

- Our understanding of snowpack processes at a point as reflected in Equations (5-26)–(5-48) is sound, and these equations can be used to simulate point snowmelt to a high degree of precision, given careful measurements

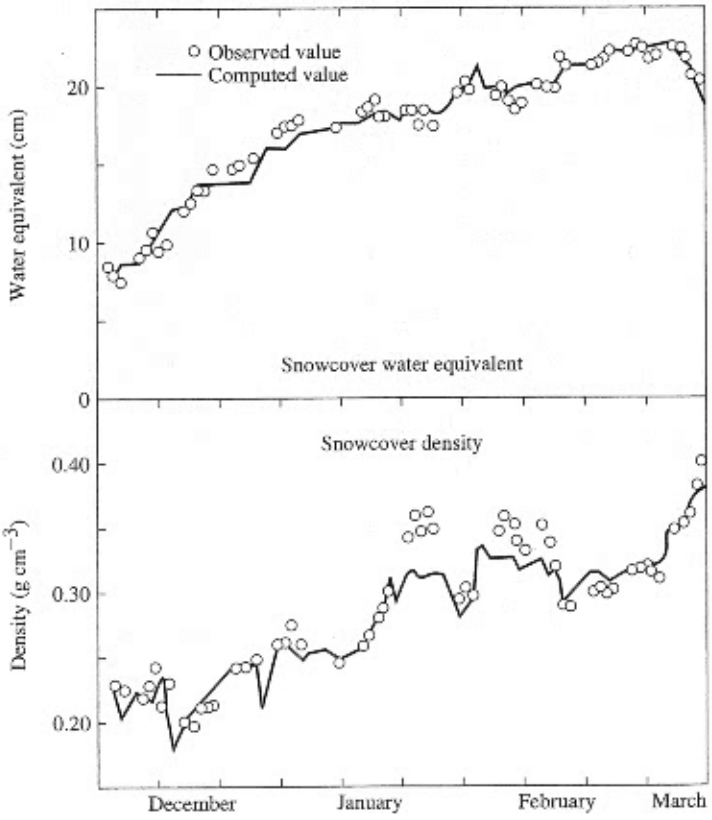

FIGURE 5-31
Comparison of observed and simulated (energy-balance model) snowpack water equivalent and density for the 1972–1973 accumulation season and warming and ripening phases of the melt season at Danville, VT. Observed values are snow-course observations. From Anderson (1976).

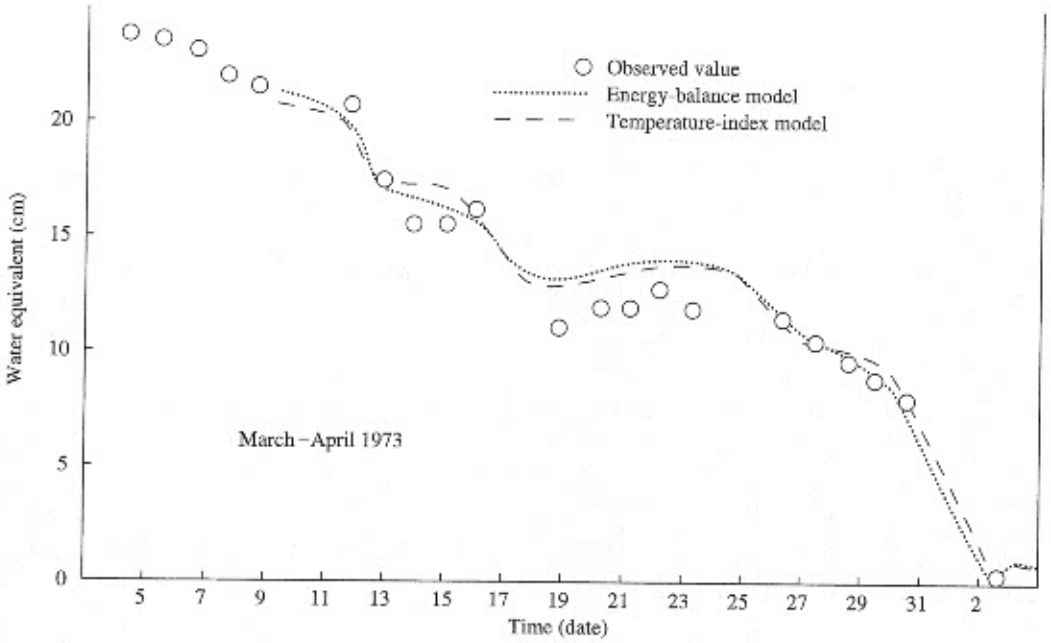

FIGURE 5-32
Comparison of observed and simulated (energy-balance and temperature-index models) snowpack water equivalent and density for the output phase of the 1973 melt season at Danville, VT. Observed values are snow-course observations. From Anderson (1976).

FIGURE 5-33
Observed vs. simulated (energy-balance model) daily water output for March and April at Danville, VT. From Anderson (1976).

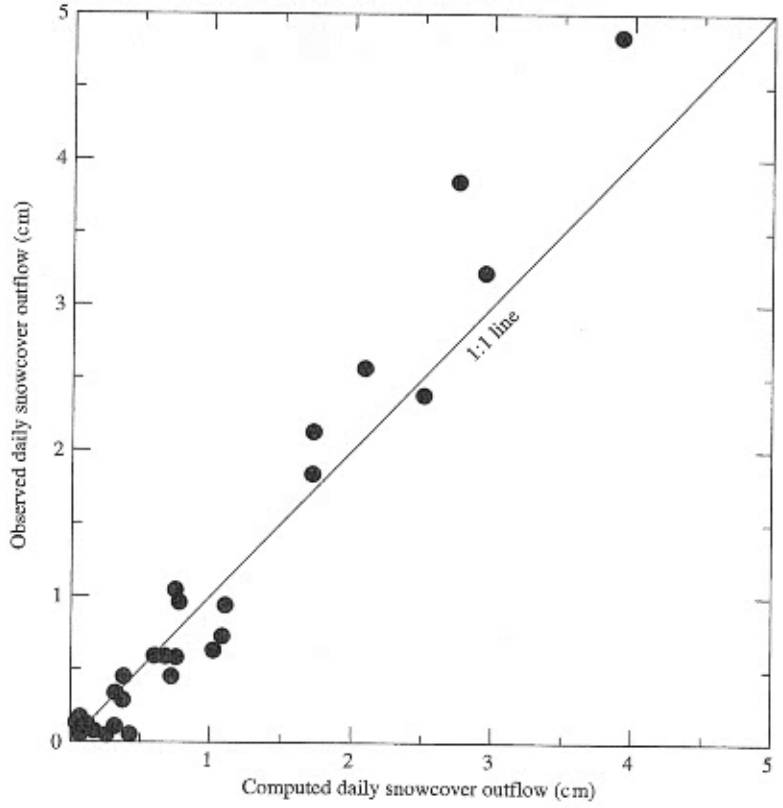

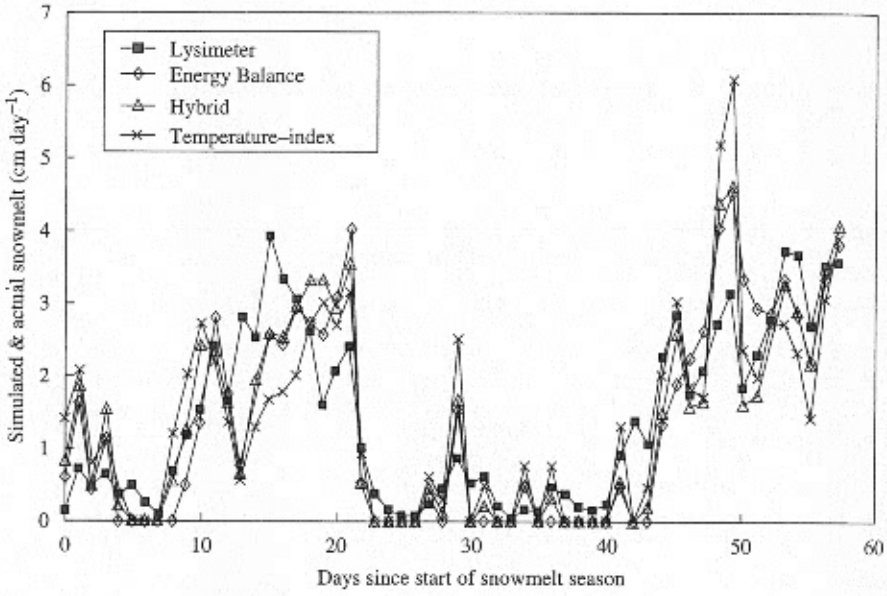

FIGURE 5-34
Daily snowmelt measured by lysimeter and simulated by the temperature-index approach, the hybrid approach, and the energy-balance approach at Weissfluhjoch, Switzerland, for the 1985 melt season. From Kustas et al. (1994); used with permission of the American Geophysical Union.

of the meteorological inputs at the point of interest.

- The temperature-index approach can provide useful estimates of daily snowmelt, but the value of the melt coefficient should reflect local conditions and seasonal changes.
- The hybrid approach appears to predict daily snowmelt with precision equivalent to that of the complete energy-balance approach and, since good estimates of the radiation components of the energy balance can usually be made with commonly available data via Equations (5-29)–(5-42), this approach will often be attractive for modeling.

5.5.2 Watershed Snowmelt Modeling

As discussed in Section 5.3.2, snowmelt is a significant contributor to runoff over much of the northern hemisphere, and changes in snowmelt runoff will be one of the most pronounced hydrologic responses to global warming. Many agencies in the countries of that region have developed models for forecasting the water supply and/or floods generated by snowmelt. The models are specifically designed for the regions of interest and the purposes of the forecasts, and hence differ in many respects. However, they all attempt to simulate the melt processes discussed in this chapter on the basis of meteorological data; to account for the typically wide range of topography, land use, and weather over watersheds; and to integrate the processes of water transmission over hillslopes and in stream channels.

Because of the wide variability of conditions, the usual sparseness of meteorological data, and the need to provide operational forecasts at relatively short time intervals (typically from 6 to 24 hr), these models make extensive use of empirical and semi-empirical relations rather than rigorous physically based models of melt and water movement. In particular, most watershed-scale models use some form of temperature-index model or hybrid approach to predict melt.

Important considerations in modeling snowmelt over large areas include the following:

1. Successfully accounting for the form of precipitation. As noted in Section 4.1.4, weather stations typically measure and report the water equivalent of precipitation without specifying whether the precipitation is in the form of rain or snow. (See Figure 4-14.) Incorrect specification of the type of precipitation will cause major errors to be made in predicting runoff and the areal extent of snow cover. This problem is exacerbated in watersheds that have a wide range of elevation.
2. Successfully accounting for the typically large range of variations in topography, elevation, and land use. This is usually accom-

plished by making adjustments in the melt factor. [See the discussion of Equations (5-59) and (5-60).]

3. Successfully accounting for spatial and temporal variations in the areal extent of snow cover. As melt proceeds, the area with snow cover decreases; over- or under-estimation of water output will be proportional to over- or under-estimation of this area. Increasingly, satellite imagery is used to update information on areal snow cover in snowmelt models.
4. Successfully accounting for the movement of water output to the watershed outlet. Various empirical and semi-empirical techniques, some of which are discussed in Section 9.6, are used for this accounting.

Dunne and Leopold (1978) summarized the equations developed by the U.S. Army Corps of Engineers for forecasting watershed snowmelt, and Anderson (1973) and Morris (1986) also examined this subject in detail. Anderson (1976) concluded that in heavily forested watersheds, a temperature-index model that includes a way to account for decreases in areal snow cover during melt should give results similar to those of an energy-balance model. However, an energy-balance model should perform better than a temperature-index model when applied to a relatively open (unforested) watershed where there is considerable variability in meteorological conditions, and in watersheds with considerable physiographic and climatic variability. Anderson found that the minimal data requirements for use of an energy-balance model are an accurate and representative estimate of incoming solar radiation, plus measurements of air temperature, vapor pressure, and wind speed.

Figure 5-35 compares streamflow from a small (8.42-km^2) watershed at the Sleepers River, VT, research site with flow predicted with a model called the Snowmelt Runoff Model (SRM) (Brubaker et al. 1996) for six seasons. Two versions of the SRM are compared, one with melt predicted by the seasonally varying temperature-index approach [Equation (5-61)] and the other with the hybrid approach [Equation (5-62)]. The hybrid approach predicted daily runoff better in only two of the six years, but predicted total runoff volume significantly better in all six years.

The most comprehensive survey of operational snowmelt-runoff models was made by the World Meteorological Organization (1986), which compared 11 temperature-index models using common data sets for six different watersheds. Rango and Martinec (1994) further compared the predictions of seven of these models for a large Canadian watershed. Blöschl et al. (1991a; 1991b) compared the performance of spatially-distributed and lumped models (see Box 2-5) in predicting snowmelt runoff from a small Austrian watershed.

Other recent studies that develop promising approaches to snowmelt that would be especially useful in predicting the effects of global warming on snow and snowmelt runoff include (1) a model of the areal depletion of snow cover in a forested catchment (Buttle and McDonnell 1987), (2) a model that simulates the growth and disappearance of the seasonal snow cover from daily air-temperature and precipitation data (Motoyama 1990), and (3) a model that uses areally averaged versions of the basic energy-balance relations to predict areal snow cover and snowmelt runoff (Horne and Kavvas 1997).

Box 5-1 summarizes the treatment of snow and snowmelt in the BROOK90 model introduced in Section 2.9.5.

5.6 WATER-QUALITY ASPECTS[9]

As described in Section 4.5, precipitation quality is determined first by the material that forms the nucleus of each raindrop or snowflake—usually sea salt, terrestrial or meteoric dust, volcanic debris, smoke particles, or various pollutants. The solubility of gases in ice is much lower than in liquid water, so gases have little effect on the quality of snowfall. However, snowflakes have large surface-to-volume ratios, and their surfaces can form hydrogen bonds with compounds in the atmosphere and are thus efficient scavengers of natural and anthropogenic atmospheric constituents as they fall.

Snowpacks in remote mountainous regions typically have pH > 5.2 and low concentrations of dis-

[9]Material in this section is based largely on the review by Hornbeck (1986); other papers on the subject can be found in Morris (1986).

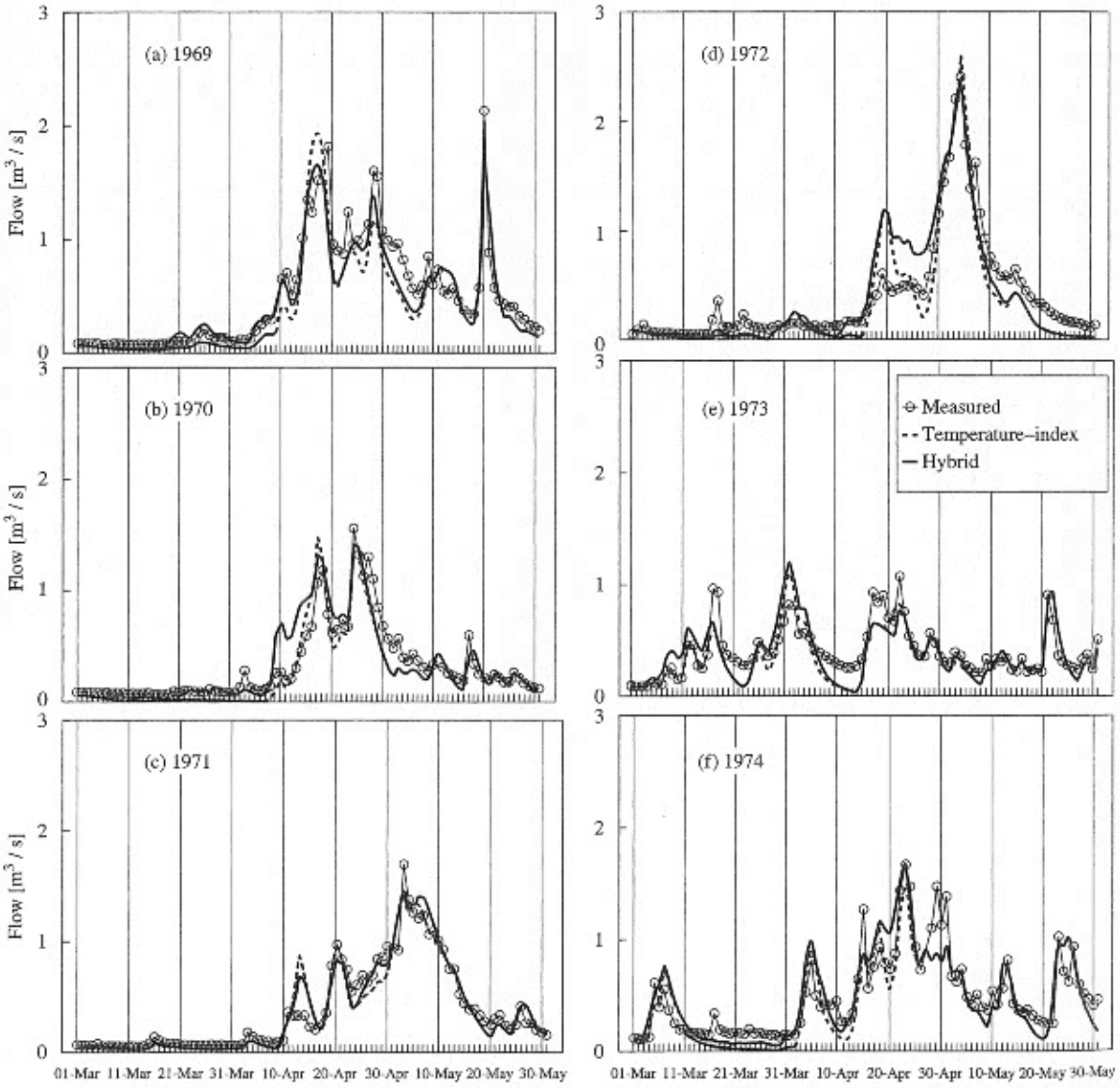

FIGURE 5-35
1969–1974 snowmelt runoff hydrographs at Sleepers River Research Watershed, VT. Open circles = measured; dashed line = temperature-index approach; solid line = hybrid approach. From Brubaker et al. (1996); used with permission.

solved ions, while those in areas affected by anthropogenic emissions have pH as low as 3.8 and ionic strengths 10 to 25 times greater. Regional variations in the relative concentration of various constituents in snow depend on storm patterns and distance from sources of contamination; on a local scale, composition can vary depending on whether the snow passed through a forest canopy or fell in the open.

After snow falls, its chemistry is further altered by natural and anthropogenic particulates that accumulate on the surface (a process called **dry deposition**) and are buried by successive snowfalls, and by rain. The percolation of rain and meltwater and their refreezing at depth further alter the distribution of chemicals in the snowpack.

At the microscopic level, the processes of freeze–thaw and vapor migration during metamor-

BOX 5-1.

Snow and Snowmelt in the BROOK90 Model

All snow quantities are expressed as water equivalents (mm), and we assume a daily time step, with the day counter indicated by i where necessary. The snow water equivalent on the ground at the end of day i is $SNOW(i)$, and the overall computations are

$$\underset{\text{Snowpack}(i)}{SNOW(i)} = \underset{=\text{Snowpack}(i-1)}{SNOW(i-1)} + \left(\underset{\text{Snow throughfall}}{STHR(i)} - \underset{-\text{Groundmelt}}{GRDMLT(i)} - \underset{-\text{Snow evaporation}}{SNVP(i)} - \underset{-\text{Snowmelt}}{SMLT(i)} + \underset{+\text{Rain on snow}}{RSNO(i)} \right) \cdot 1\ \text{day}. \quad \textbf{(5B1-1)}$$

These quantities are determined as follows:

1. Daily precipitation (*PREC*) is input to the model. Snowfall (*SFAL*) is computed as

$$SFAL = SNOFRC \cdot PREC, \quad \textbf{(5B1-2)}$$

where the algorithm for determining the fraction of precipitation that is snow (*SNOFRC*) is described in Box 4-1.

2. Snow throughfall (*STHR*) is found as

$$STHR = SFAL - SINT. \quad \textbf{(5B1-3)}$$

The snowfall interception rate, *SINT*, is determined by two input parameters that describe the canopy density: the leaf-area index, *LAI*, (one-sided surface area of leaves divided by ground area) and the stem-area index, *SAI*, (projected cylindrical surface area of stems and branches divided by ground area). (See Section 7.5.2.) The relation is

$$SINT = (FSINTL \cdot LAI + FSINTS \cdot SAI) \cdot SFAL, \quad \textbf{(5B1-4)}$$

with default values $FSINTL = 0.04$ and $FSINTS = 0.04$. Interception continues at this rate until the canopy-storage capacity, *INTSMX*, is reached where

$$INTSMX = CINTSL \cdot LAI + CINTSS \cdot SAI. \quad \textbf{(5B1-5)}$$

Default values are $CINTSL = 0.6$ and $CINTSS = 0.6$.

3. The groundmelt rate *GRDMLT* is a parameter with a default value of 0.35 mm day^{-1}.
4. Snow evaporation/condensation (*SNVP*) is computed from the latent-heat exchange relation [Equations (5-46) and (D-42)], with roughness and zero-plane displacement heights determined by the vegetation height and density.
5. Snowmelt is computed by a temperature-index approach that accounts for slope, aspect, and vegetative density. If air temperature $TA > 0$ °C, the energy available for melting, *SNOEN* (MJ m^2 day^{-1}), is

$$SNOEN = MELFAC \cdot 2 \cdot DAYLEN \cdot SLFDAY \cdot TA \cdot \exp(LAIMLT \cdot LAI + SAIMLT \cdot SAI), \quad \textbf{(5B1-6)}$$

where *MELFAC* is a melt factor for a 12-hr day on a horizontal surface with no plant cover, with a default value of 1.5 MJ m^{-2} day^{-1} K^{-1}. *DAYLEN* is the fraction of the day the sun is above the horizon, which is calculated from relations given in Section E.2.2, and *SLFDAY* is the ratio of extraterrestrial solar radiation on the sloping watershed to that on a horizontal plane (the "slope factor," f_{sh}, discussed in Section E.2.4). The last two terms are empirical adjustments for vegetation density, where $SAIMLT = -0.5$ and $LAIMLT = -0.2$ are the default values. Partitioning of *SNOEN* is discussed in Step 8.

6. If some of the precipitation is rain, the rain throughfall *RTHR* is added to the snowpack. If $TA < 0$ °C, some of the rain is refrozen and warms the snowpack. Any remaining liquid water is used to increase the liquid-water content *SNOWLQ* up to a maximum value *MAXLQ* ($= \theta_{res}$), which has a default value of 0.05; this quantity = *RSNO*. The remaining water infiltrates into the soil.
7. After *STHR* is added to the snowpack, if $TA < 0$°C, the cold content, *CC*, of the new snowpack is computed as

$$CC(i) = CC(i-1) - TA \cdot CVICE \cdot STHR \cdot 1\ \text{day}, \quad \textbf{(5B1-7)}$$

where *CVICE* is the volumetric heat capacity of ice.

8. After *GRDMLT* and *SNVP* are removed, the energy available to produce a temperature change or melt, *EQEN*, is computed as

$$EQEN = (SNOEN + RTHR \cdot RMAX(TA, 0) \cdot CVLQ)/LF, \quad \textbf{(5B1-8)}$$

where *RMAX*(*TA*,0) is the rain temperature (the maximum of *TA* and 0 °C) and *CVLQ* is the heat capacity and *LF* the latent heat of freezing of water. If *EQEN* < 0, the energy is used to refreeze any liquid water and then increase *CC*. If *EQEN* > 0, the energy is used first to reduce *CC* and then to produce melt, *SMLT*.